1994-07-01

Transports and budgets of volume, heat, and salt from a global eddy-resolving ocean model

McCann, M.P.; Semtner, A.J. Jr.; Chervin, R.M.

Springer

Journal Name: Climate Dynamics; Journal Volume: 10; Journal Issue: 1-2; Other Information: PBD: Jul 1994
http://hdl.handle.net/10945/60993

Climate Dynamics (1994) 10:59–80

Climate Dynamics

Transports and budgets of volume, heat, and salt from a global eddy-resolving ocean model

Michael P McCann[1], **Albert J Semtner, Jr**[2], **Robert M Chervin**[3]

[1] Naval Postgraduate School, Code 51, Monterey, CA 93943, USA
[2] Naval Postgraduate School, Code OC, Monterey, CA 93943, USA
[3] National Center for Atmospheric Research, Boulder, CO 80307, USA

Received: 30 November 1992/Accepted: 28 May 1993

Abstract. The results from an integration of a global ocean circulation model have been condensed into an analysis of the volume, heat, and salt transports among the major ocean basins. Transports are also broken down between the model's Ekman, thermocline, and deep layers. Overall, the model does well. Horizontal exchanges of mass, heat, and salt between ocean basins have reasonable values; and the volume of North Atlantic Deep Water (NADW) transport is in general agreement with what limited observations exist. On a global basis the zonally integrated meridional heat transport is poleward at all latitudes except for the latitude band 30°S to 45°S. This anomalous transport is most likely a signature of the model's inability to form Antarctic Intermediate (AAIW) and Antarctic bottom water (AABW) properly. Eddy heat transport is strong at the equator where its convergence heats the equatorial Pacific about twice as much as it heats the equatorial Atlantic. The greater heating in the Pacific suggests that mesoscale eddies may be a vital mechanism for warming and maintaining an upwelling portion of the global conveyor-belt circulation. The model's fresh water transport compares well with observations. However, in the Atlantic there is an excessive southward transport of fresh water due to the absence of the Mediterranean outflow and weak northward flow of AAIW. Eddies in the mid-latitudes act to redistribute heat and salt down the mean gradients. Residual fluxes calculated from a sum of the computed advective (including eddies), forced, and stored fluxes of heat and salt represent transport mostly due to vertical sub-grid scale mixing processes. Perhaps the model's greatest weakness is the lack of strong AAIW and AABW circulation cells. Accurate thermohaline forcing in the North Atlantic (based on numerous hydrographic observations) helps the model adequately produce NADW. In contrast, the southern ocean is an area of sparse observation. Better thermohaline observations in this area may be needed if models such as this are to produce the deep convection that will achieve more accurate simulations of the global 3-dimensional circulation.

Correspondence to: MP McCann

1 Introduction

The global ocean circulation plays a major role in determining the Earth's climate. In the simplest sense, the ocean absorbs heat in the tropical latitudes and transports it poleward. Satellite measurements show that the ocean's contribution to this heat transport is nearly equal to that of the atmosphere (Carissimo et al. 1985). Two principle mechanisms for oceanographic heat transport are wind-driven gyre circulation and thermohaline-driven deep ocean overturning. The characteristics of these large scale processes are often determined by smaller scale processes such as mesoscale eddies, diffusion, and convection. Strong currents, such as the Gulf Stream, exchange energy with mesoscale eddies and small-scale convective chimneys drive the deep ocean circulation. In the authors' opinion, any realistic formulation of the 3-dimensional global ocean circulation should include a representation of these meso- and small-scale processes over a global domain. Current technology makes possible explicit representation of meso-scale processes in global ocean models, yet important small-scale processes, such as deep convection, must still be parameterized.

Efforts at constructing a global oceanic circulation budget were begun by Stommel and Arons (1960). Their work provides the framework for modern oceanographic thought on inter-basin abyssal circulation. They assume that there are two sources of abyssal water (water below 3000 m), one in the North Atlantic and the other in the Weddell Sea. A second assumption is that there is uniform upwelling of water in all ocean basins. Using observations placed under dynamical constraints, they outline the flow of abyssal water and give estimates for North Atlantic Deep Water (NADW) flow of 20 Sv (1 Sverdrup $= 10^6$ m^3/s) and for

bottom water flow originating in the Weddell Sea of also 20 Sv. Residence time in the deep ocean is estimated to be between 200 and 1800 years. This general view has survived despite a great deal of observational and modeling studies done during the last 30 years.

The World Ocean Circulation Experiment (WOCE) is designed to expand our observational base and provide data that will help improve models (Woods 1985). The 5-year program will essentially give a snapshot of present ocean conditions along basin-wide cruise tracks; satellite observations will provide ocean surface height and wind forcing data. Even with this ambitious plan, the in situ observations will be sparse and the remotely-sensed data will provide information only at the surface of the ocean. Modeling studies are essential in integrating sparse observations into a consistent picture of the ocean's circulation and in predicting variability that may lead to climate change. Modeling and being able to predict ocean circulation is a chief aim of WOCE. It has been only in the last 15 years that mathematical modeling of the global ocean circulation has allowed us to integrate our observational and theoretical knowledge of ocean circulation. And it has only been in the last five years that computer technology has been available to begin to model the general circulation of the global ocean with resolved eddies (Chervin and Semtner 1990). Verifying such model runs is difficult because of limited observational data; one intent of this paper is to distill the results of an eddy-resolving calculation into gross figures that are suitable for comparison with other global measures of volume, heat, and salt (or fresh water) transport. A still open question in climate modeling is "what is the role of meso-scale ocean variability in influencing Earth's climate?" Since this is a model that begins to resolve ocean eddies in all the major ocean basins, it can be used for baseline research into this question.

2 Modeling background

Mathematical modeling of the global ocean with realistic coastlines and bathymetry was first accomplished by Cox (1975). Using the Bryan (1969) model, Cox integrated the primitive equations of motion on a 2 degree horizontal grid with 9 levels in the vertical. This model, referred to as the Bryan and Cox model, is a general tool for modeling ocean circulation in irregular domains having realistic coastlines and bottom topography. For more on the history and formulation of global ocean modeling see Semtner (1986a, b).

Chervin and Semtner (1990) describe a formulation of the Bryan and Cox model that exploits the vector and multitasking features of modern supercomputer architectures. This revised model realistically simulates the global ocean circulation on a 0.5 degree horizontal grid with 20 levels in the vertical. An initial 20 year run of this model forced with annual-mean winds, temperature, and salinity is described by Semtner and Chervin (1988). The change from Laplacian to biharmonic closure of the frictional and diffusive parameterizations at year 18 of the simulation allowed for the spontaneous generation of mesoscale eddies. Starting at year 20, instantaneous fields of the prognostic variables were written at 3 day intervals to a history tape archive and the model was run for another 2.5 years with annual-mean forcing. These last 900 days have been divided into three 300-day segments from which statistical products have been computed. After 22.5 years, the external forcing was changed from climatological annual-mean to monthly-varying, and the simulation was continued for another 10 years. Statistical products have also been computed for each of these last 10 years. This paper concentrates on the latter 5 years of this 10 year period. The ocean's simulated general circulation from this extension of the model is described by Semtner and Chervin (1992).

This paper summarizes the model's climatological transports of volume, heat, and salt across idealized boundaries of the world's oceans. In addition, the external forcing and storage within each basin is examined. How these changed when the forcing was changed from annual-mean to seasonally-varying is also examined. The meridional transports of heat and salt are compared with measurements as a test of the model. Section 3 describes the partitioning of the major ocean basins and how the statistics were calculated. Section 4 discusses the model's volume budget, section 5 the heat budget, and section 6 the salt and fresh water budgets.

3 Calculation of the fluxes

The oceans are divided into eight regions representing the major ocean basins as shown in Fig. 1. The Atlantic and Pacific are split into a North, a Tropical and a South basin with inter-basin boundaries at 15°N and 15°S. The Indian is split into a North and a South basin with a boundary at 25°S. Each basin, in turn, is divided into 3 layers: (1) the surface layer from 0 m to 25 m, (2) the thermocline layer from 25 m to 710 m, and (3) the deep layer from 710 m to the bottom. These layers were chosen because of the different forcing used in each layer during the simulation. The surface layer's temperature and salinity were restored to the climatological values (Levitus 1982) on a monthly time scale, while the thermocline layer (except within 10 degrees of the north and south boundaries where temperature and salinity were restored to climatological values on a three-year time scale) was unforced after year 10 of the integration. The deep layer was continually restored to climatology on a 3-year time scale. Surface layer horizontal transports represent the total Ekman transport as the wind is applied at only this level and not in a variable depth mixed layer. The 9 model levels within the thermocline layer have the greatest degree of mesoscale variability because it would be maximal there anyway and because there is no restoring there during most of the simulation. The deep layer contains much of the global thermohaline circulation, yet still retains mesoscale variability as it is only weakly constrained to climatological observations.

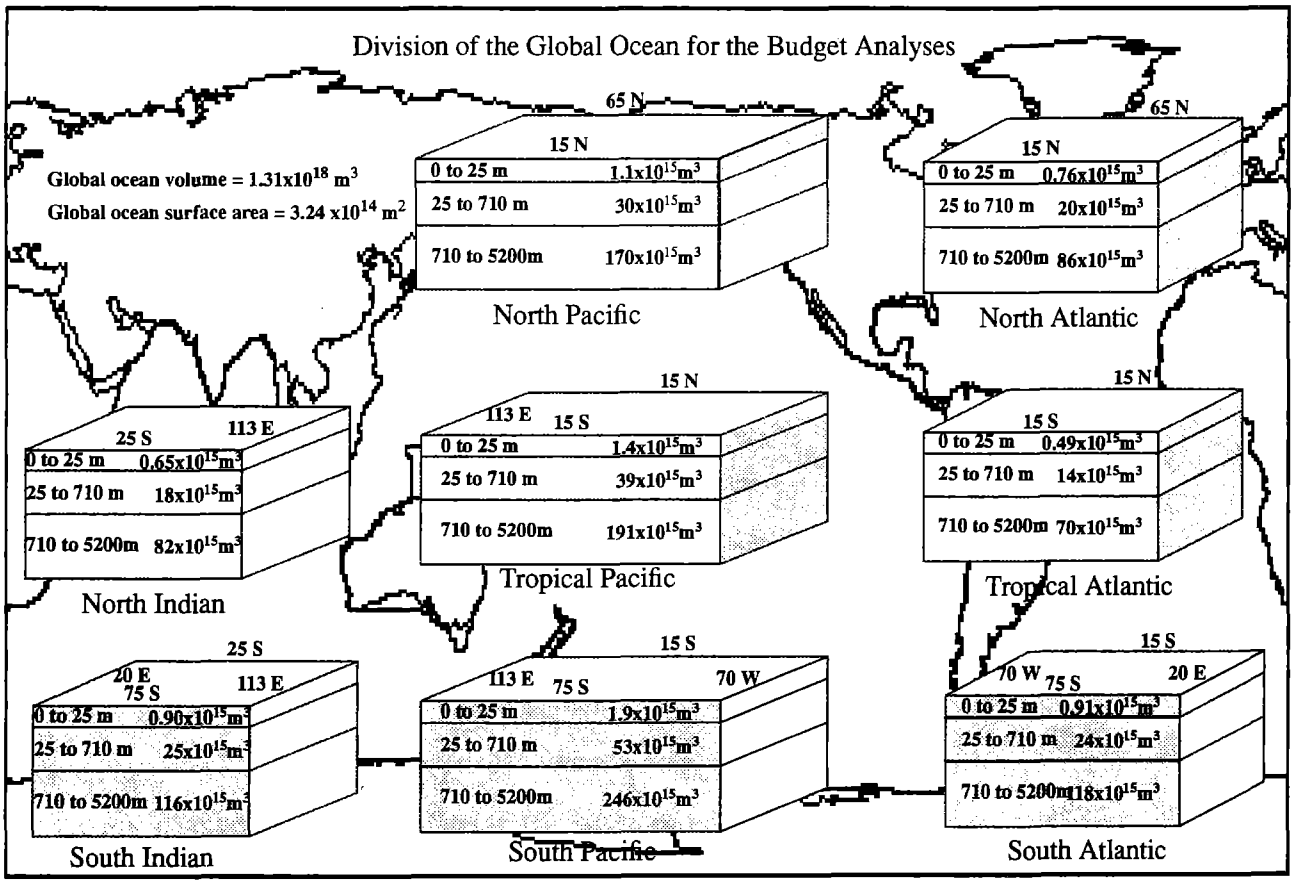

Fig. 1. Division of the global ocean for the budget analyses. The 8 boxes are split into 3 layers whose lateral and depth boundaries are indicated. The volume of each layer is also noted

We have computed the transports of volume, heat, and salt across all inter-box faces. External thermohaline forcing was computed by subtracting the observed annual-mean climatological values of temperature or salinity from the 30-day mean and yearly mean simulated values. The appropriate forcing factors, (1 month)$^{-1}$ for the surface layer, and (3 years)$^{-1}$ for the deep layer and the wall forcing in the thermocline layer, were applied to compute the external forcing of heat and salt. Storage of heat or salt was computed from the trends seen in our samples from the annual-mean and seasonal forced model runs. The samples are the three 300-day means from the annual-mean forced run, the years 5, 6, and 7, and the years 8, 9, and 10 from the seasonally forced run. The three sets of data allow for statistically reasonable comparisons, although the latter two data sets yield nearly identical numbers, for example, when contrasted with the annual-mean forced results. In addition, we also use data from a mean over the last five years for computing meridional transports and implied surface fluxes. As the model is well equilibrated by year five of the seasonal run, intercomparisons between the 5-year and 3-year means are valid. We did not directly compute the diffusive and convective fluxes, but instead estimated them by summing the known fluxes into each box and assuming that the residual represents these sub-grid scale processes.

4 The model's volume budget

The model's transport stream function is shown in Fig. 2. Figure 2a is the mean transport over the seasonally forced years 6 through 10, and Fig. 2b is an instantaneous snapshot from October of year 10. The ocean's mean currents and regions of mesoscale variability can be seen in these figures. Boundaries for the basins used in the budget analysis are indicated in these figures.

Figure 3 shows the computed volume transports across each face of our "boxed" ocean. The results from both the annual-mean forced model run and the seasonally forced run are indicated in this Figure. The numbers in the plain font are from the annual-mean case and the numbers in bold are from years 5, 6, and 7 of the seasonal run. The only major difference between the transports of these two cases is in the North Atlantic where the deep water formation in the seasonal run is about 20% larger. The deep water transport is greater in the latter case because the ocean responds to the annual-minimum temperature (and annual-maximum salinity) rather than to the annual-mean of the external thermohaline forcing. In the North Pacific, a reversal of thermocline and deep layer exchange took place: the annual-mean downwelling of 1.7 Sv changed to an upwelling of 0.3 Sv. The consistency between the two cases in the rest of the interfacial transports indicates that a high degree of equilibration was attained

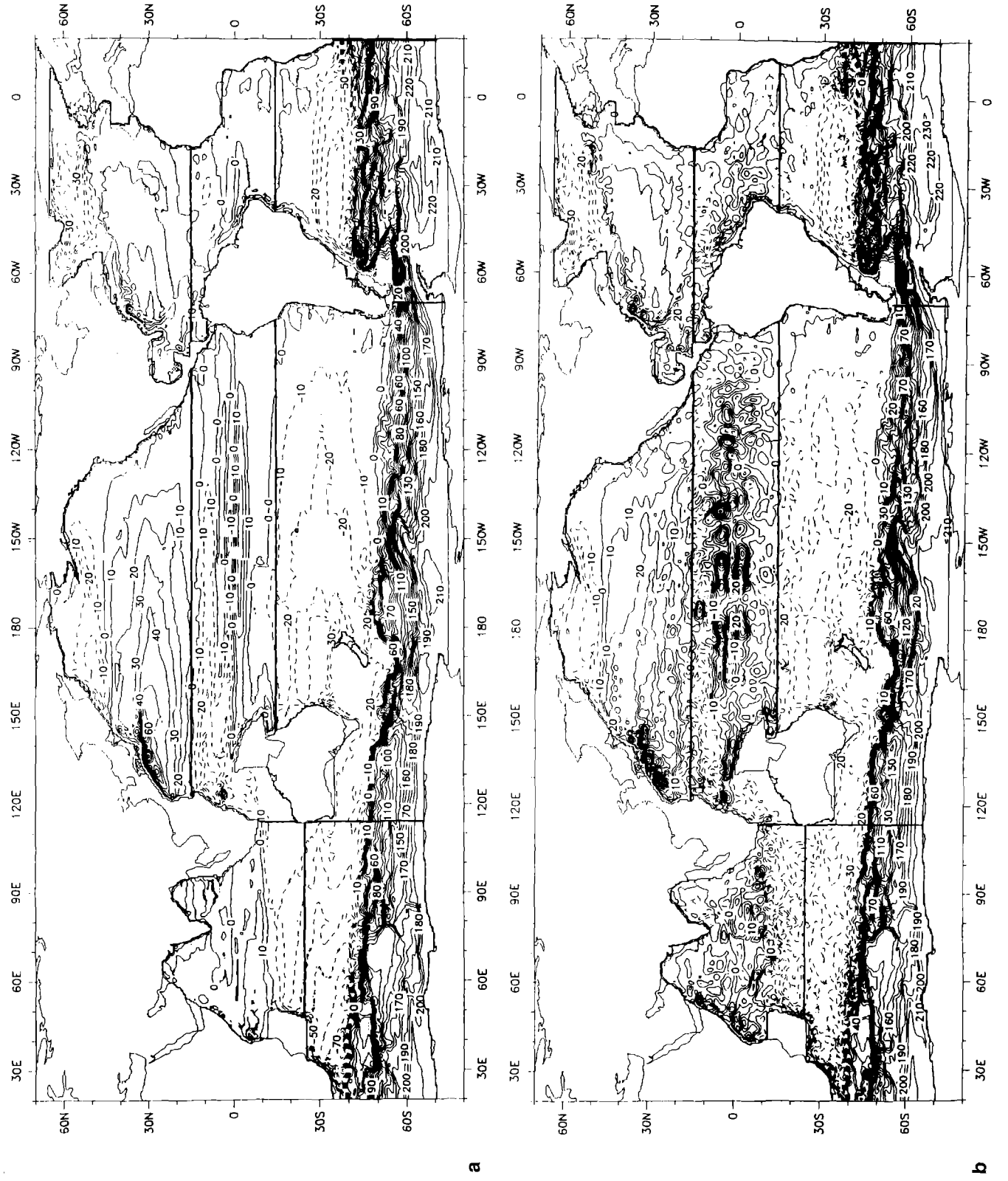

Fig. 2. Volume transport stream function for **a** the mean of years 6 through 10 of the seasonal run and **b** a snapshot from early October of year 10 of the seasonal run. Boundaries for the basins used in the budget analysis are indicated

during the annual-mean forced run. The volume transports from years 8, 9, and 10 are nearly identical to the transports from years 5, 6 and 7.

The pattern of the global circulation seen in Fig. 3 shows that in the North Atlantic, water flows south in the thermocline and deep layers with a total flow of 14.1 Sv (seasonal years 5, 6 and 7). In contrast, the North Pacific has no deep equatorward flow. The deep

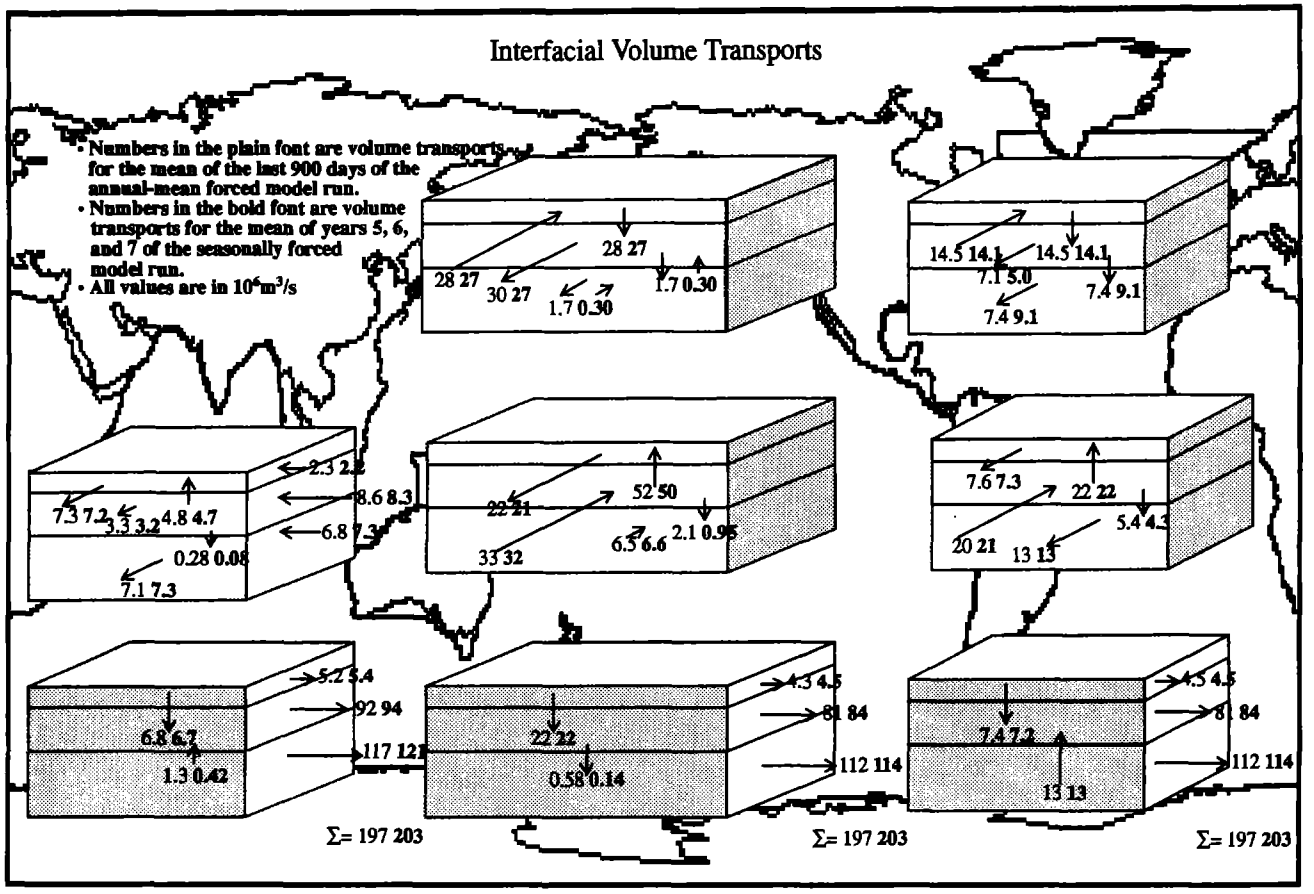

Fig. 3. Interfacial volume transports in Sv (10^6 m^3/s). Numbers in the *plain font* are from the annual-mean forced model run and the numbers in the *bold font* are from the seasonally forced model run. The total zonal transports across 113°E, 70°W, and 20°E are shown next to the summation sign near the bottom of the figure

layer transport from the Tropical Atlantic into the South Atlantic is 13 Sv. An equivalent 13 Sv upwells into the thermocline layer of the South Atlantic and is the largest of all the vertical transports. This upwelling is necessary to balance the mass transport in the Atlantic (which has a closed boundary at 65°N), but it swamps any signature of intermediate or bottom water formation in the South Atlantic basin. The Weddell Sea (where most of AABW is formed) is a small part of the South Atlantic, and bottom water formation there is seasonal, episodic, and has sub-grid length scales. Our averaging over the whole South Atlantic and over several years probably masks any downwelling that occurs there. We should also note that the model's convective adjustment process causes vertical mass transport via mixing. Unfortunately, a measure of this mixing was not recorded in the history tape archive, so these effects are not explicitly included in the large scale vertical advective transports shown in Fig. 3.

The spreading of deep water from the North Atlantic into the rest of the world's oceans is difficult to interpret from Fig. 3. Our averaging over large areas hides the true nature of these flows, which usually exist as narrow boundary currents. In contrast, this basin-scale averaging helps distinguish regional differences in the large scale flow. Semtner and Chervin (1992) describe a narrow deep western boundary current of NADW in the Atlantic. This water flows via the Antarctic Circumpolar Current (ACC) into the Indian and Pacific Oceans, where according to the theory of Stommel and Arons (1960) it should uniformly upwell.

The vertical transports between the thermocline and deep layers are near zero everywhere, except in the three basins of the Atlantic Ocean. Near the surface, we see a pattern that is consistent with the equatorial divergences and mid-latitude convergences of the global wind forcing field. Ekman pumping in the Equatorial Pacific, with (as is shown later) augmentation by eddy convergence of buoyancy, causes 50 Sv of upwelling into the surface layer. Upwelling into the surface layers of the Atlantic and Indian amounts to 22 Sv and 4.7 Sv. The extra-tropical Pacific basins have downward vertical transports of order 20 Sv and the extra-tropical Atlantic and Indian have downwelling that is order 10 Sv. Though largely due to Ekman dynamics and the basin's long zonal extent, the 50 Sv of upwelling in the tropical Pacific is considerable and must play a role in the thermohaline circulation.

The zonal transport through the Indonesian Passage from the tropical Pacific to the Indian Ocean may be critical in determining how the surface water in the North Atlantic is replenished. As discussed by Gordon (1986) and Semtner and Chervin (1988), this passage is

Table 1. Layer residence times (in years)

Basin	Annual-mean forcing			Seasonal forcing: Years 5, 6, and 7		
	Surface	Therm	Deep	Surface	Therm	Deep
North Atlantic	1.66	43.00	365.7	1.71	44.3	297.9
Tropical Atlantic	0.698	16.46	172.4	0.698	17.5	164.0
South Atlantic	2.41	7.61	30.0	2.43	7.32	29.3
North Pacific	1.26	31.69	3050.0	1.31	34.77	17667.3
Tropical Pacific	0.860	19.74	702.8	0.897	20.93	800.1
South Pacific	2.22	14.54	66.0	2.28	14.33	64.4
North Indian	2.84	65.34	364.9	2.90	68.24	353.8
South Indian	2.43	8.47	31.1	2.42	8.24	30.4

a conduit for the global conveyor-belt circulation. Variations in this transport may influence global climate patterns. As seen in Fig. 3, the throughflow is 17.7 Sv for the annual-mean case and 17.8 Sv for years 5, 6, and 7 (17.5 Sv for years 8, 9, and 10) of the seasonal case. Gordon (1986) discusses the observational estimates of Indonesian throughflow; they range from Fine's (1985) estimate of 5.1 Sv in the upper 300 m to Piola and Gordon's (1984) estimate of 14 Sv. Estimates from other numerical modeling studies include 7 Sv (Kindle et al. 1987), 16 ± 4 Sv (Godfrey 1989), and 17 Sv (Masamichi and Welsh 1990). Seasonal and interannual variability in the model's Indonesian throughflow is discussed by Long (1990). Long finds the weakest transport is 15.70 Sv in December and the strongest is 21.28 Sv in April, corresponding to a strengthening of the North Equatorial current (NEC) in the Pacific. Because the model is forced with identical monthly forcing from year-to-year we would not expect much interannual variability. The largest interannual variability, computed from a 5-year sample, is a 1.02 Sv deviation from the mean. This throughflow in our budget is at the high end of previously published values, perhaps because of the simplified geometry of the Indonesian archipelago.

Another area where zonal transport can be compared to observations is in the ACC. The transports at Drake's Passage and south of Africa are both 197 Sv with annual-mean forcing and 203 Sv with seasonal-varying forcing. Current meter and hydrographic data taken from the Drake Passage show that the ACC transport is between 117 and 144 Sv (Whitworth et al. 1982). Hydrographic measurements taken south of Africa give a similar value of 140 Sv (Whitworth and Nowlin 1987). As discussed by the FRAM Group (1991), general circulation z-coordinate models have difficulty computing bottom pressure drags and torques in the presence of topography. Both the high resolution FRAM model (1/2 degree in longitude, 1/4 degree in latitude) and the 2 degree resolution global model by Cox (1975) give ACC transports around 200 Sv. Alternatively, standard hydrographic measurements or current meter arrays may underestimate the total flow because of undersampling. The ACC circulation seen in this and the FRAM model consists of narrow meandering currents which may be missed in a hydrographic survey.

Estimates of residence times within each box are obtained by dividing the volume of the box by the total flow through the box. Table 1 shows the residence times in years for each layer in each basin for the annual-mean forced run and for years 5, 6, and 7 of the seasonal forced run.

The most significant change from the annual-mean case to the seasonal forced case is in the deep North Atlantic where residence times decreased by 20% to 298 years. An apparently more dramatic change occurs in the deep North Pacific where the residence time increased nearly 6 times. Because these time-scale calculations neglect convection and diffusion, the advective flow through a layer may not give an accurate measure of the true residence time, especially in the deep North Pacific where advection is very small. Nevertheless, the residence time of the deep North Pacific is significantly greater than the other deep basins which illustrates its isolation from the major paths of the global ocean circulation. The effects of rapid transport by the ACC can be seen in the southern hemisphere basins where the largest residence time (from the seasonal case) is 64 years in the South Pacific.

5 Heat budget

The temperature at 37.5 m is shown for an instant in October of year 10 in Fig. 4. Mean gradients and eddy features can be seen in relation to the boundaries of the basins. Figures 5, 6, and 7 show the heat budgets for the annual-mean forced run and for the two samples from the seasonally forced run. For each layer in each basin the contributions to the heat budget by external forcing, advection, and storage are shown. Summing these terms gives a residual transport which represents sub-grid scale transport processes. These residuals, which must be considered in order to have a balanced budget, are shown within parentheses in the figures.

We can infer a great deal about the model's performance from these figures. In general, the budgets show a warming of surface equatorial waters and ad-

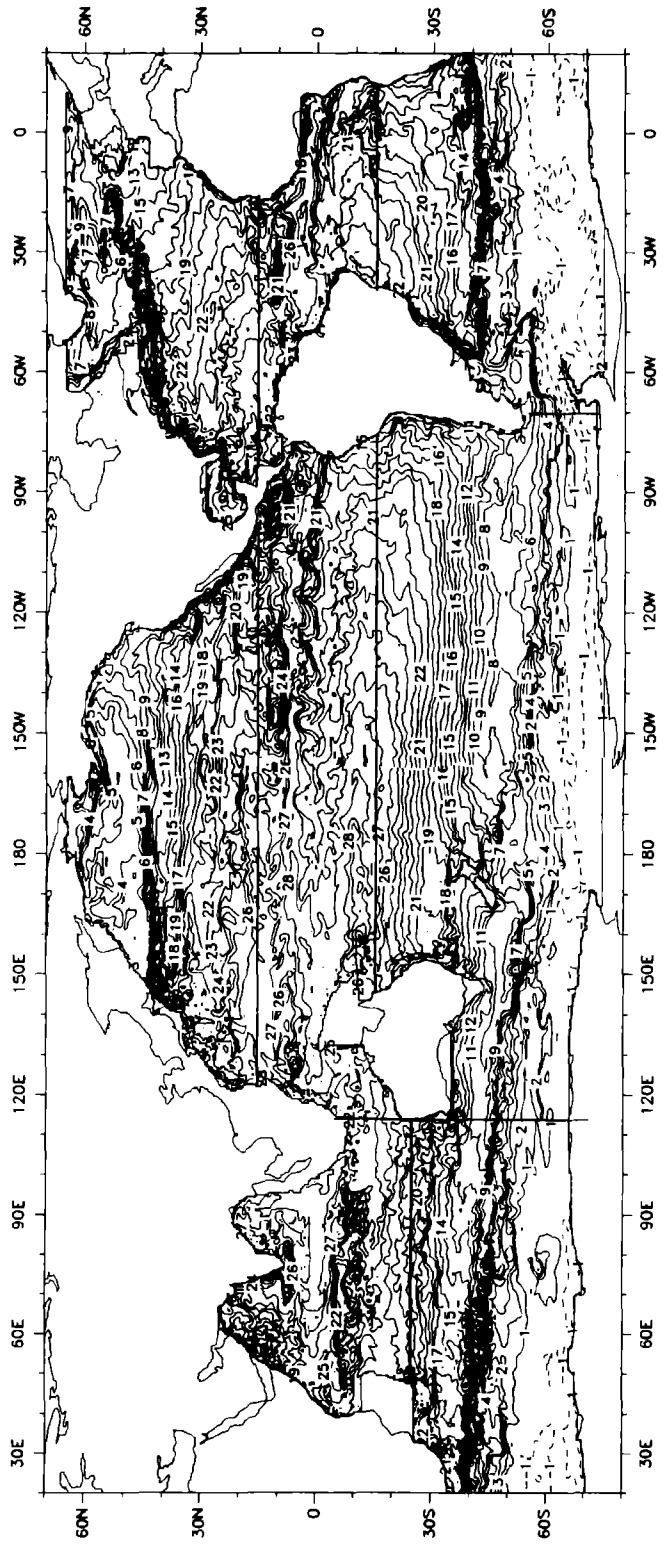

Fig. 4. Temperature at 37.5 m for an instant in early October of year 10 of the seasonal run. Contour interval is 1 Deg C. Boundaries for the basins used in the budget analysis are indicated

vective transport of these waters towards the poles. Heat is returned to the tropics by equatorward transport in the thermocline layer. External forcing of the deep layer, which substitutes for poorly resolved convective processes, is greatest in the three basins (North Atlantic, South Atlantic, and South Pacific) where deep water is formed. The largest residual fluxes are in the surface and thermocline layers and represent mainly vertical mixing which takes place between these two layers.

External forcing

Fluxes of heat and fresh water between the atmosphere and the ocean are accomplished through the forcing of the model's surface layer toward observed climatological values of surface temperature and salinity. In effect, the model ocean is overlain by an atmosphere with prescribed seasonally varying fluxes. This pseudo-atmosphere also accounts for the transport of heat and fresh water between the ocean basins. Weak diagnostic forcing is applied below the surface layers of the model to help maintain the deep circulation and to augment poorly resolved convection.

Using the basin-wide areal averages (Figs. 5, 6, and 7), we can quantitatively assess how the model reacted when the external forcing was changed from annual-mean to seasonal. In the annual-mean run, the ocean north of 15°N was cooled at a rate of 213 TW (TW $= 10^{12}$ W), the southern basins were warmed at a rate of 878 TW (Fig. 5). After the seasonal cycle was spun up, the northern hemisphere cooling increased to 694 TW and the southern hemisphere warming decreased to 459 TW (Fig. 6). These changes are mainly due to the increased formation of NADW during the seasonal run. Though the onset of seasonal forcing lowered the atmospheric warming of the ocean's surface below 15°S, it did not provide for enough convection to increase bottom water formation significantly in the southern hemisphere.

Lateral boundary forcing is applied to the thermocline layer within 10 degrees of the northern and southern boundaries. This forcing is a relaxation toward climatological temperature and salinity with a three year time constant. In the North Atlantic this forcing is two times larger than in any other region. This external cooling of 171 TW (Fig. 6) acts as a proxy for the missing Arctic Ocean. At all boundaries, the magnitude of wall forcing decreased when the forcing changed from annual-mean to seasonal.

External forcing in the deep layers is of the same order of magnitude as surface layer forcing in the North Atlantic, South Atlantic, and South Pacific basins. (It is an order of magnitude less in the remaining 5 basins.) The ocean's cold deep water is formed in the North Atlantic, the Weddell Sea, and the Ross Sea. The model's diagnostic forcing corrects for inadequate deep convection by removing heat from the deep layers of these basins. Except for North Atlantic basin (which can have deep water inflow from the Arctic), this deep layer forcing has no physical analog – it is an artificial adjustment of heat content based on the model's tendency to drift away from climatology. External forcing removes heat from the deep layer of each basin but the Tropical Pacific. Basins where deep water

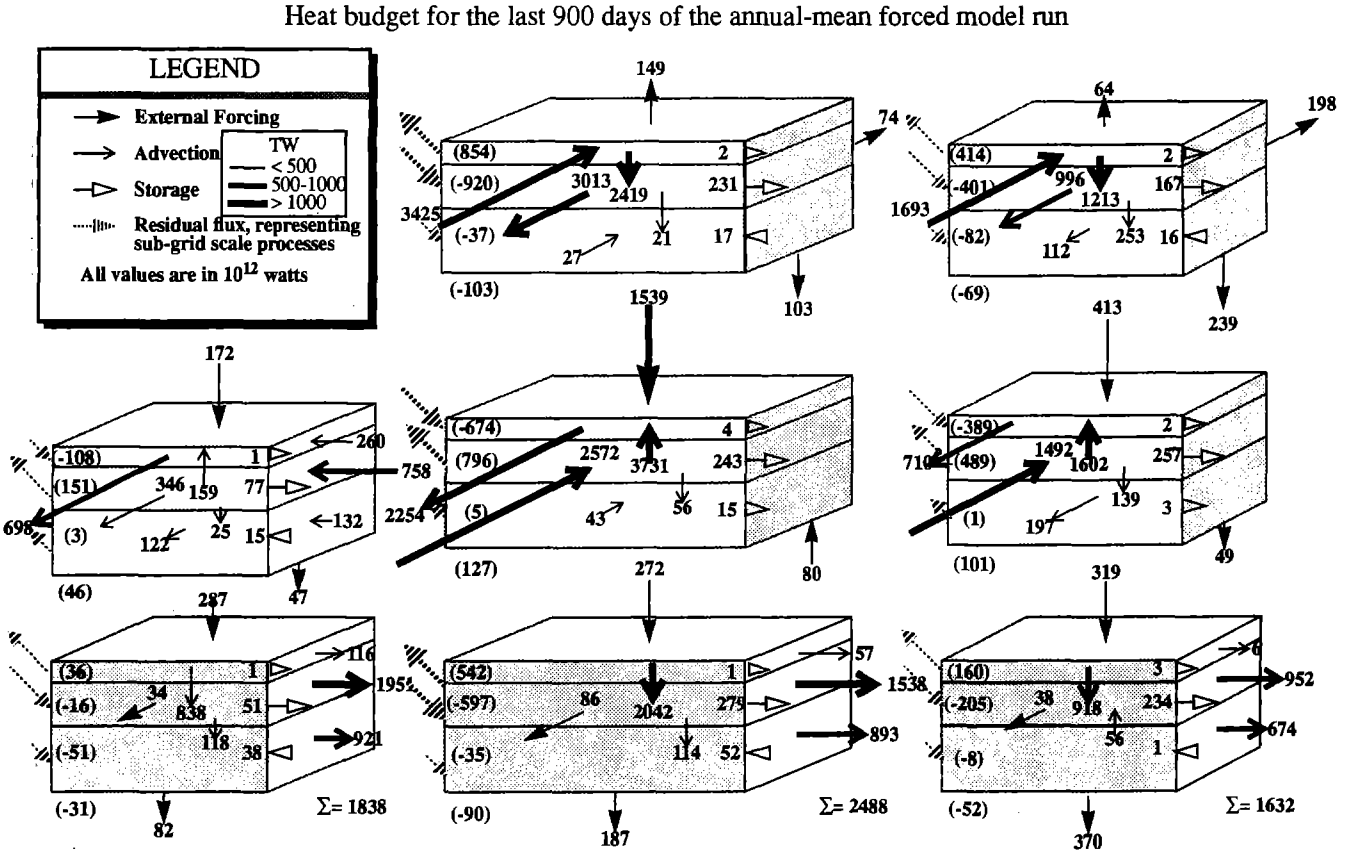

Fig. 5. Heat budget in TW (10^{12} watts) for the last 900 days of the annual-mean forced model run. *Solid filled arrows* represent external forcing, *plain arrows* represent advective transport between layers, *open filled arrows* represent the storage within the layer, and the *broken arrows* represent the sub-grid scale transports into or out of the layer. *Wide arrows* indicate transports greater than 1000 TW, medium-sized arrows are for transports between 500 and 1000 TW, and thin arrows indicate transports less than 500 TW. The total zonal transports across 113° E, 70° W, and 20° E are shown next to the summation sign near the bottom of the figure

forms (the North Atlantic and the South Atlantic) consistently have the largest removal of heat (Figs. 5, 6, and 7). These fluxes, which are order 300 TW, indicate the magnitude of additional deep convection that is required for the model to properly form deep water.

Heat storage

Storage of heat is represented by the *open-filled arrows* in Figs. 5, 6, and 7. An *arrow* leaving the box shows the removal of heat from the box's *budget*; in other words it indicates a rise in temperature for the box. The unforced thermocline layers have the most heat storage with a relatively high positive temperature trend in all basins during the annual-mean forced run. With the change to seasonal forcing these trends decrease. Seasonal forcing causes the surface layer temperature to decrease below the annual mean during the winter months. This leads to proper seasonal ventilation of the thermocline layers and hence a lowered temperature trend.

The thermocline layer warming is consistent with the net positive external forcing applied at the surface, walls, and within the deep layer. The total external forcing for years 5, 6, and 7 is 612 TW, for years 8, 9, and 10 it is 679 TW. This later amount of forcing would warm the global ocean at a rate of 0.039° C/decade. The net surface imbalance averages about only 2 W/m^2, which is a small percentage of the total surface flux and far smaller than the 10–20 W/m^2 discrepancies seen in coupled air-sea models.

Heat advection

As mentioned above, heat flows away from the equatorial regions in the surface layer and returns in the thermocline layers. An exception is in the Indian Ocean where there is about 300 TW poleward transport across 25° S within the thermocline (Figs. 6 and 7). From Fig. 7, the total temperature transport through the Indonesian archipelago is 1077 TW and the total transport from the North Indian into the South Indian is a comparable 1148 TW. So the North Indian is a conduit for heat that comes from the equatorial Pacific and goes into the South Indian.

The advective heat transports shown in Figs. 5, 6, and 7 are most readily interpreted when they are summed on an interface that has zero net mass flux, or if

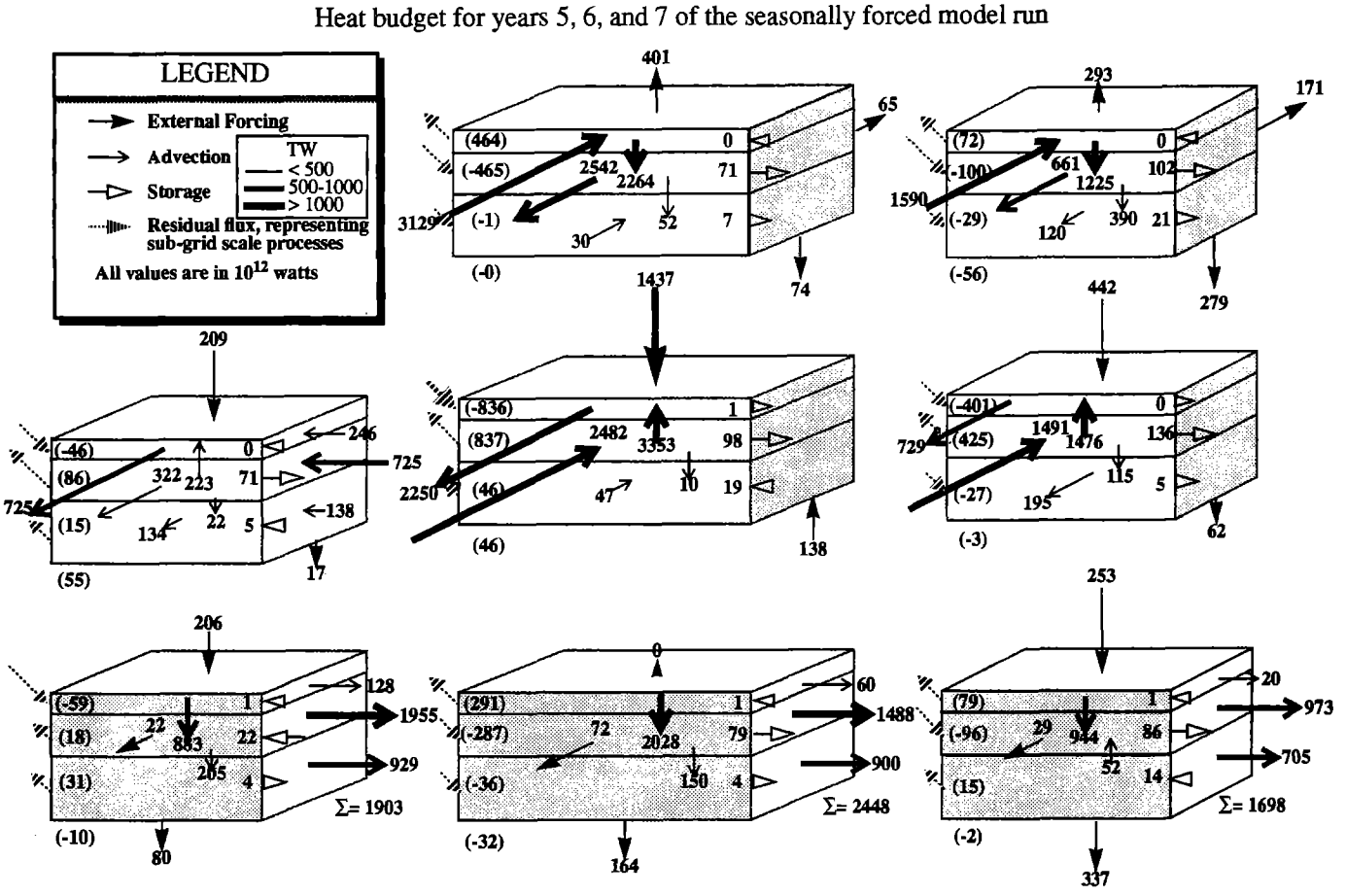

Fig. 6. Heat budget in TW (10^{12} watts) for years 5, 6, and 7 of the seasonally forced model run. Same conventions as Fig. 5

they are compared with the heat transport on another interface that has an identical mass flux. Three of the latter interfaces are those separating the three major oceans at 113 E, 70 W, and 20 E. The respective eastward transports are 1903 TW, 2448 TW, and 1698 TW (shown next to the summation sign in Fig. 6). The differences in these transports gives us the heat gained or lost in each ocean: the Indian loses 205 TW, the Pacific loses 545 TW and the Atlantic gains 750 TW. (The differences for years 8, 9, and 10 are respectively 151 TW, 534 TW, and 685 TW.) This model's Atlantic heat gain compares well with Hastenrath's (1982) estimate of 690 TW.

Residual fluxes

The residual flux (representing subgrid scale transport) for a layer is obtained by summing the computed advective, forced, and storage fluxes. It is indicated for each layer in Figs. 5, 6, and 7 by a number enclosed in parentheses. The *broken arrows* next to these numbers are a graphic representation of the additional fluxes that are needed to balance the budget. These residual flux arrows point either into or out of the layer; they do not point towards a particular layer because they may go to any adjacent layer. The calculation of these residuals does not allow the exact source or sink to be specified.

These residual fluxes are attributed to sub-grid scale mixing processes that have been parameterized in this simulation, namely diffusion and convection. Horizontal mixing is accomplished by biharmonic diffusion, and vertical mixing is parameterized in terms of the Richardson number as in Pacanowski and Philander (1981), as well as by convective adjustment. A simple case of how the residual fluxes balance between adjacent layers can be seen in the North Pacific of the seasonal years 5, 6, and 7. The sum of the known fluxes (advection, forcing and storage) into the surface layer is 464 TW. The sum of the known fluxes into the thermocline layer is −465 TW. The budget for these layers can be nearly balanced by assigning a transport of 464 TW from the surface to the thermocline. This is a plausible downward heat flux due to sub-grid scale mixing processes. This assumed flux is in the same direction as the advective flux between these layers and about 20% of its magnitude. Since the residual fluxes for the surface and thermocline layers in most of the other basins are nearly the same magnitude but have opposite signs, we may assume that vertical mixing between these layers accounts for much of the residual flux in these layers.

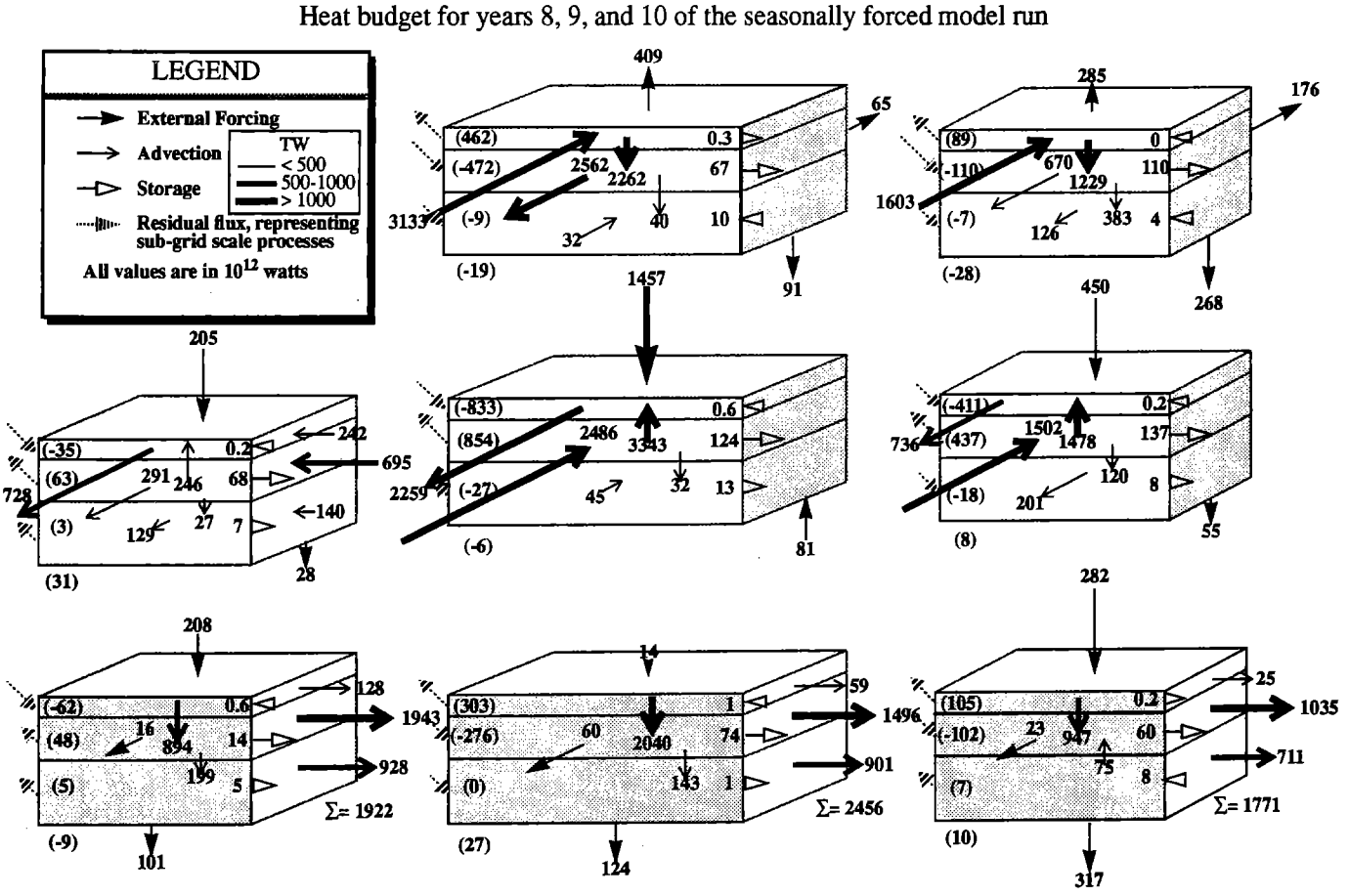

Fig. 7. Heat budget in TW (10^{12} watts) for years 8, 9, and 10 of the seasonally forced model run. Same conventions as Fig. 5

The value in parentheses outside of the lower-left corner of the box is the total residual flux for each basin. It represents the sub-grid scale horizontal transports among the basins and probably includes errors introduced by approximations that were made. (For instance, our calculation of storage is approximate, as it is a difference between the mean temperatures of the first and last years of the sample.) To see how the basin residuals represent horizontal diffusive transport, consider the North and South Indian basins. Figure 4 shows a strong meridional temperature gradient along the boundary separating these basins. Horizontal diffusion across this boundary may account for some of the 31 TW surplus in the north and for most of the 9 TW deficit in the south (Fig. 7). As a measure of the relative error in our method we can sum the residuals for all of the basins: from the annual-mean run the total is −71 W, from years 5, 6, and 7 it is −2 TW, and from years 8, 9 and 10 it is 14 TW. These errors are small in comparison to the model's major transports, which are order 1000 TW.

Meridional heat transport and implied heat fluxes

With T and V representing the instantaneous 3-day temperature and meridional velocity, and an overbar ($\overline{\ }$) representing a 5-year mean of these values, then the 5-year mean of the meridional heat transport may be decomposed into mean and fluctuating components:

$$\rho C_p \overline{VT} = (\rho C_p)\overline{(\bar{V}+V')(\bar{T}+T')} = (\rho C_p)(\overline{\bar{V}\bar{T}} + \overline{V'T'})$$

The first term on the right is the meridional transport due to *mean* currents and the second term on the right is the meridional transport due to *eddies*. Figure 8a shows the vertically integrated meridional transport of heat summed zonally over the global ocean from the last 5 years of the seasonal run. The *solid curve* is the total transport ($\rho C_p \overline{VT}$), which includes the transport due to eddies, and the *dashed curve* is the eddy transport ($\rho C_p \overline{V'T'}$).

The maximum total northward transport of 1.37 PW (10^{15} watts) at 14°N is about half of that derived from satellite and radiosonde observations (Carissimo et al. 1985) but about the same order as that computed from hydrographic observations and surface heat budget analyses (Hastenrath 1982). In the southern hemisphere the peak poleward transport is 0.7 PW at 12°S. An interesting feature occurs in the region from 45°S to 30°S where the heat transport is equatorward with a maximum of 0.3 PW at 40°S. This feature may not have appeared in non-eddy-resolving simulations of the global circulation (e.g. Maier-Reimer and Mikola-

jewicz 1989) because in these models lateral diffusion dominates, forcing the poleward transport of heat. Semtner and Chervin (1992) discuss how the anomaly in this simulation may not be a real feature of the ocean circulation and might be due to weak Antarctic Bottom Water (AABW) formation or due to poor resolution of high-latitude eddies which would better mix heat across fronts of the ACC. If the model's transport of AABW was increased by 20 Sv, and it transported water that was on average 5 degrees colder than the surrounding water then poleward heat transport in the 45°S to 30°S latitude band would increase by 0.4 PW, nullifying the equatorward transport. We may need to improve both the explicit formation of deep water and the representation of high-latitude eddies if we are to have meridional heat transport that is antisymmetric about the equator, as is seen in indirect measurements (Carissimo et al. 1985).

There is a possibility that equatorward heat transport may be a real feature of the southern ocean. A direct measurement of the ocean heat transport at 30°S gave a northward transport of 1.15 to 2.27 PW (Bennett 1978). Bennett's measurement greatly exceeds the model's transport (which is near zero at 30°S), but along with these model results, it raises a question of whether the ocean does transport heat equatorward in the southern hemisphere. If the equatorward heat transport is real, then it may be because of the geometry or phenomena in a particular basin, such as the South Atlantic where heat is added at a high southern latitude. If there is not enough poleward transport in the Pacific and Indian Oceans, then the northward transport in the South Atlantic (of order 0.5 PW in Fig. 8b) may show up as an equatorward transport in summation over the global ocean. Another possibility is that strong westerlies in this latitude belt drive a shallow circulation cell which transports warm surface water equatorward. In Fugio and Imasoto's (1991) diagnostic calculation of circulation in the Pacific, the heat transport is less than 0.15 PW poleward between 30°S and 45°S. Direct measurements in the South Pacific (Wunsch et al. 1983) indicate negligible poleward heat transport at 28°S and 43°S. So the South Pacific's poleward heat transport may not be large enough to counteract the anomalous equatorward transport in the South Atlantic. Whether the global ocean's equatorward heat transport is real or not awaits more extensive direct measurements as well as further examination of this and other model data sets.

Eddies transport a maximum 1.28 PW toward the equator at 3.5°N (Fig. 8a). The large eddy heat transports in the tropics are strongly associated with tropical instability waves (e.g. Legeckis 1977) which are stronger in the Pacific than in the Atlantic (Figs. 8b and 8c). The tropics, more than any other latitude belt, contain the largest eddy heat transports. This may be a result of the model's 0.5 degree resolution which gives better resolution of mesocale disturbances at low latitudes than at high latitudes. Bryan (1991) compares a hierarchy of models of increasing resolution and concludes that eddies do not change the poleward transport of

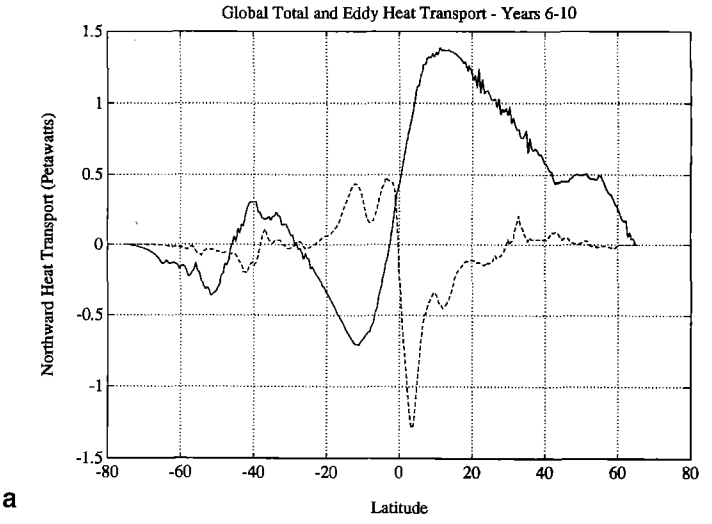

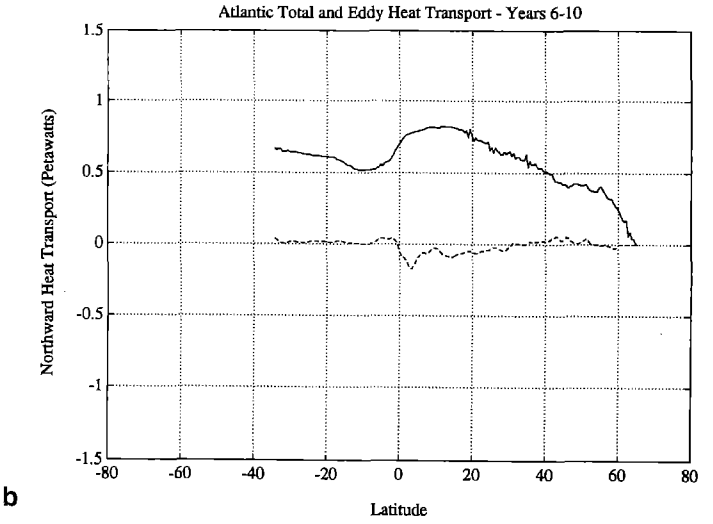

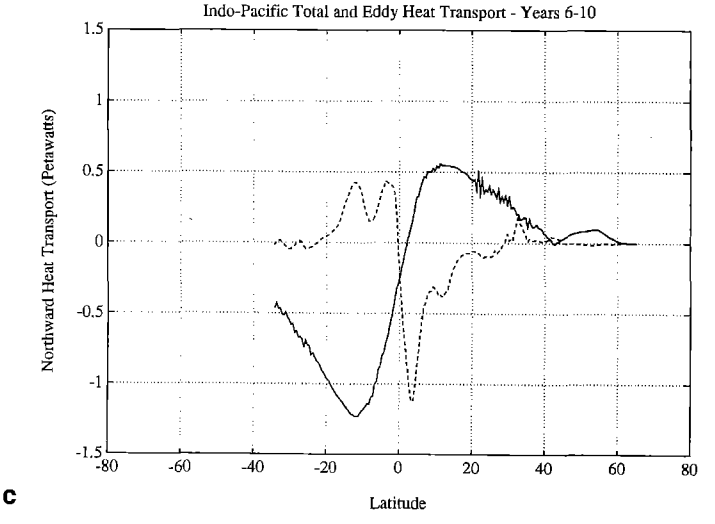

Fig. 8. Depth and latitude integrated total (*solid*) and eddy (*dashed*) heat transport in PW (10^{15} watts) over **a** the global ocean, **b** the Atlantic ocean, and **c** the Indo-Pacific ocean

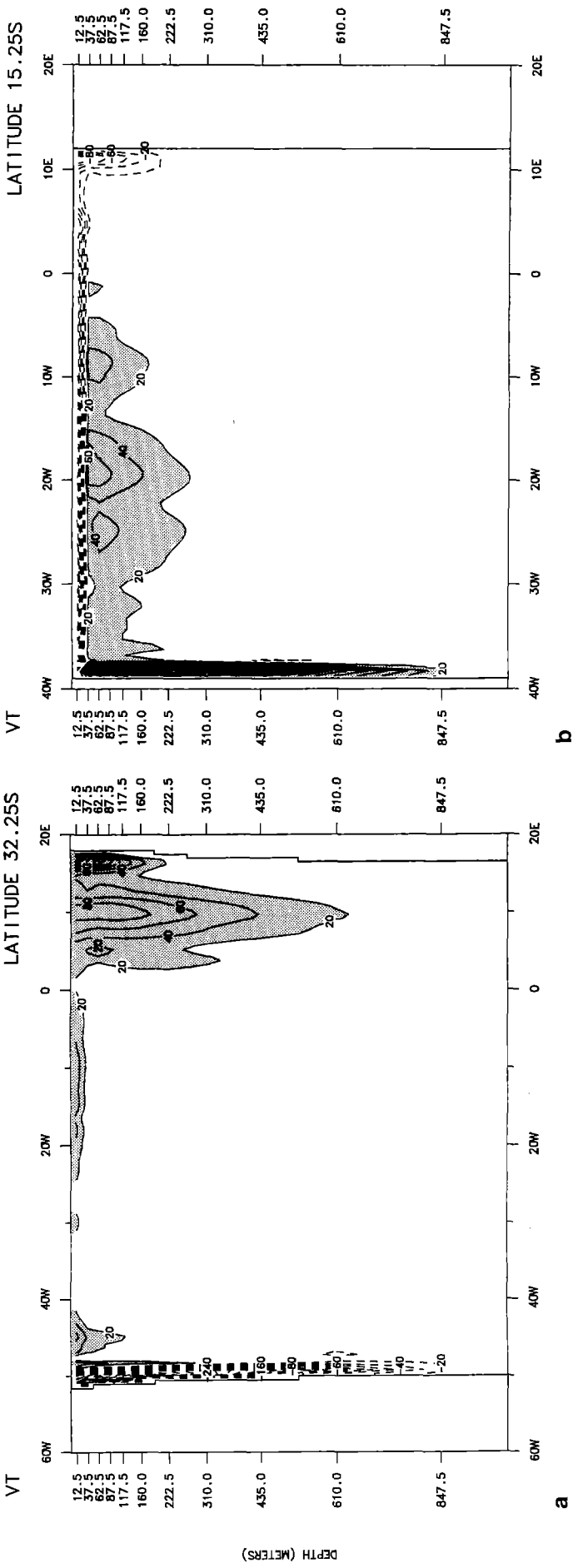

heat. Instead, they generate mean flows which tend to cancel the fluxes caused by eddies. This direct interaction between eddy and mean flow is supported by Figs. 8a, 8b, and 8b where there is virtually no correlation between the total and eddy heat transports. Eddies, as we see later, may still influence global oceanic heat transport by mixing buoyancy and aiding vertical transport along critical routes of the thermohaline circulation.

Figure 8b shows the total (*solid*) and eddy (*dashed*) meridional heat transport summed zonally over the Atlantic Ocean. Total heat transport is northward at all latitudes with a peak of 0.82 PW at 13.5 N. The South Atlantic heat transport is anomalous in that it flows to the north rather than poleward. Gordon (1986) states that this anomaly is due to the introduction of warm water that enters the Atlantic via a branch of the Agulhas current that does not curl back into the Indian Ocean as part of the Agulhas retroflection. Computer animations of the temperature field from this model indeed show that warm-core eddies are shed off the Agulhas Current which then move to the west-north-west across the South Atlantic. (Copies of this video in NTSC or PAL format may be obtained by contacting one of the authors.) The FRAM group (1991) estimates that these eddies are responsible for a heat flow of 0.2 PW into the Atlantic.

As an example of how heat is transported by currents in the South Atlantic, Fig. 9 shows the meridional temperature transports at 32°S and 15°S (*shading* indicates northward transport). The transport east of the prime meridian at 32 S adds 1.82 PW to the Atlantic and the transport west of the prime meridian (mostly due to the western boundary current along the coast of South America) takes away 1.18 PW (Fig. 9a). Summing the two gives a net heat gain for the Atlantic of 0.64 PW. The net heat gain at 15°S (Fig. 9b) is a similar 0.57 PW, but the current structure is quite different. The region of equatorward transport has moved west and has concentrated much of its flow into a western boundary current. Northward temperature transport is confined mostly to the upper 25 m, the sum of which is 0.73 PW, as indicated by the surface layer transport shown in Figs. 6 and 7.

At 25°N the total northward heat transport is 0.67 PW, somewhat less than the 1.2±0.3 PW computed from hydrographic measurements at this latitude (Hall and Bryden 1982), but within the seasonal range of

Fig. 9a, b. Zonal section of the meridional total temperature transport in units of deg C cm/s in the Atlantic. Northward transport is *shaded*, southward transport is shown with *dashed contours*. To convert to Watts/m^2 multiply by 41800. **a** At 32°S; heat added to the Atlantic between 0°E and 20°E (the region of spin-off eddies from the Agulhas) amounts to 1.82 PW. Heat taken away by the western boundary current between 60°W and 0°E amounts to 1.18 PW, leaving a net gain of 0.64 PW. **b** At 15°S; northward temperature transport is concentrated in a western boundary current. Southward transport is in the surface layer and in a poleward flowing eastern boundary current. The Atlantic gains 0.57 PW at this latitude

0.57 to 0.75 PW calculated by a higher resolution model of the Atlantic Ocean (Bryan and Holland 1989). Both models transport NADW at a rate of 15 Sv, which is still significantly less than other estimates which range around 20 Sv (e.g. Stommel and Arons 1960). The disagreement between the models and the observation indicate that underestimated overturning transport may cause less than observed meridional heat transport. We should also note that increased horizontal model resolution does not necessarily improve overturning circulation.

Eddy heat transport throughout most of the Atlantic is small compared to the total transport. However between 1°N and 5°N there is equatorward eddy transport, with a maximum of 0.17 PW at 3°N. This relatively weak transport, compared to that in the Indo-Pacific (Fig. 8c), is consistent with the model's weaker tropical instability wave activity in the Atlantic. The effective heat flux due to eddies in the Atlantic (Fig. 10b) is order 100 W/m^2. Bryan and Holland's (1989) 1/3 degree in latitude, 2/5 degree in longitude model of the North Atlantic does give higher mid-latitude eddy transports (0.1 PW poleward at 40°N) than this 1/2 degree model (0.05 PW poleward at 43°N), but does not show the eddy heat convergence at the equator.

Figure 8c shows the total and eddy heat transports for the Indo-Pacific ocean (bounded by the 20°E and 70°W meridians). The total circulation transports twice as much heat southward at 12°S (1.2 PW) as it does northward at 13°N (0.55 PW). This is most certainly because of the large southward heat transport that takes place in the Indian Ocean (Fig. 7 and Hastenrath 1982). The eddy heat transport within 20 degrees of the equator is of the same order as the total transport; the convergence of eddy heat transport at the equator is 200 W/m^2 (Fig. 10c). This zonal average over the Indo-Pacific basin matches fairly well the value of 245 W/m^2 computed by Bryden and Brady (1989) from upper-level current meter observations taken in the Pacific at 152°W and 110°W. This convergence of heat at the equator by eddies may be a vital mechanism for warming an upwelling portion of the global conveyor-belt circulation.

Derived total and eddy heat fluxes for the global, Atlantic, and Indo-Pacific oceans (computed by differentiating the transports with respect to latitude and then dividing by the width of the basin) are shown in Fig. 7. A 2-degree latitude filter was applied to suppress noise that results from the differencing operation. The filter was not applied within 1 degree of the equator for the eddy transports in order to preserve the magnitudes of the equatorial convergences. Solid curves indicate that atmospheric surface heat fluxes that are computed from the total heat transport and are hence required by the model's circulation. A downward heat flux of 50 W/m^2 is a plausible value for the heating of the ocean by the atmosphere at the equator (Hastenrath and Lamb 1977). At mid- and high-latitudes the global ocean (Fig. 10a) loses heat to the atmosphere except around 40–50°S and 45–50°N. The highest heat flux out of the ocean is over 100 W/m^2 at

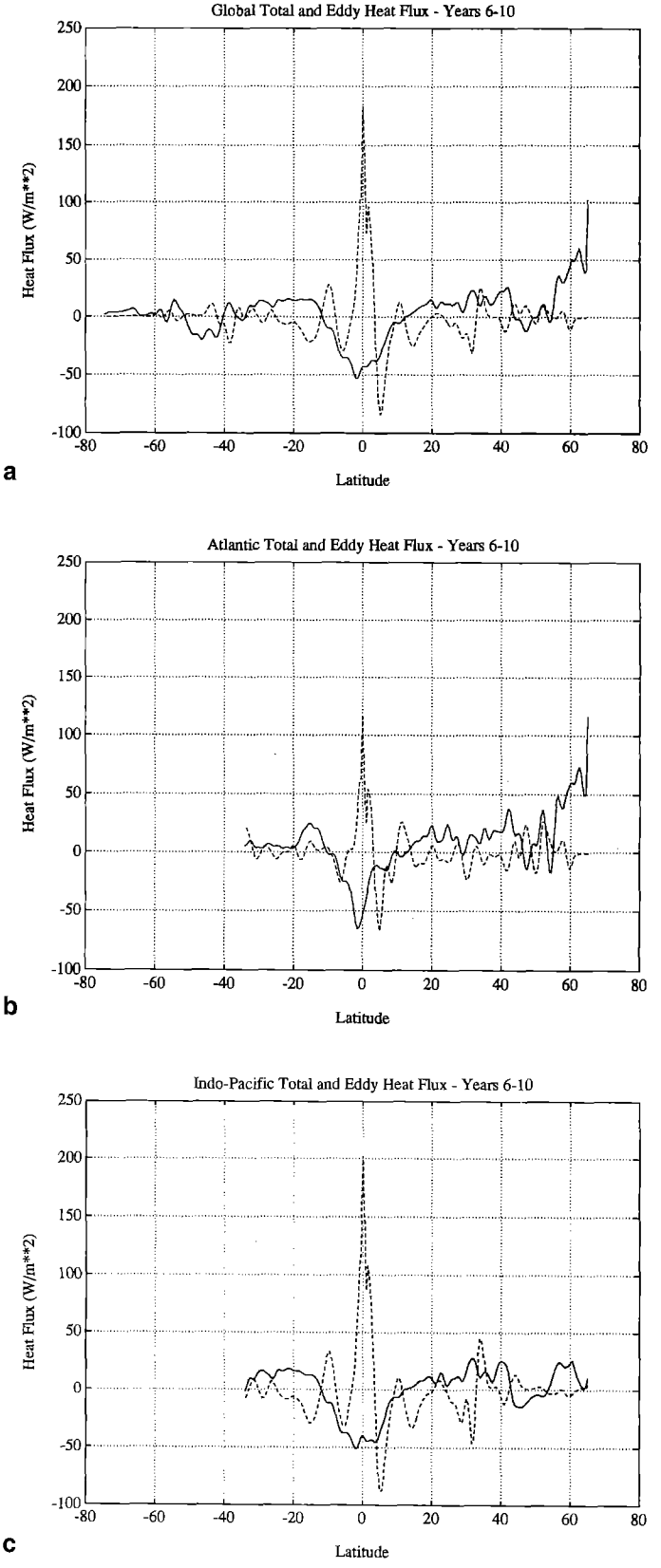

Fig. 10. Derived total (*solid*) and eddy (*dashed*) heat flux in W/m^2 over **a** the global ocean, **b** the Atlantic ocean, and **c** the Indo-Pacific ocean. The *solid line* represents the surface heat flux required by the model's circulation (positive values mean the ocean heats the atmosphere) and the *dashed line* represents the effective heat flux due to eddies (positive values mean that the eddies converge heat in the ocean)

65°N and most of this flux takes place in the Atlantic (compare Figs. 10b and 10c). The relative importance of eddy heat flux (*dashed curves*) is easily seen in these figures.

Effective eddy fluxes are of the same order as total surface fluxes at all latitudes and tend to be out of phase, especially in the 30–50 latitude bands. The out-of-phase fluctuations indicate the role that eddies play in the mid-latitudes. By bringing cold water to the surface, upwelling in a cyclone increases atmospheric heat input and the horizontal temperature gradients caused by the upwelling allow instabilities where eddies grow. The eddies then act to redistribute heat down-gradient. Likewise, downwelling in an anticyclone increases surface temperatures and eddies act to diverge heat away from the centers of downwelling. These fluctuations have latitudinal scales of 300 Km – the characteristic length scale of Gulf Stream rings. It will be interesting to see the effect of eddies when global models are able to resolve motions at scales smaller than the mid-latitude radius of deformation.

Salt budget

The salinity at 37.5 m is shown for an instant in October of year 10 in Fig. 11. Mean gradients and fronts can be seen in relation to the boundaries of the basins. Figures 12, 13, and 14 show the salt budgets for the annual-mean forced run and the seasonally forced run. In general, evaporation exceeds precipitation in the high latitude basins (indicated by the external forcing of salt into the surface) and precipitation exceeds evaporation in the equatorial basins. Of course in the real ocean, fresh water, and not salt, is transported across the air-sea interface. For the transports and fluxes shown in Fig. 12 through 15, the equivalent fresh water transport can be estimated by dividing the salt transport by a reference ocean salinity of 35×10^3 g/m^3 and reversing the sign. For instance, the global salt transport of 28 Gg/s (1 Gg/s $= 10^9$ g/s) across the equator (Fig. 15a) is equivalent to a southward fresh water transport of 0.8×10^6 m^3/s. This equivalence is valid because the net mass flux across this interface is zero.

External forcing

The most notable surface layer forcing is in the South Indian where there is 12 Gg/s transport of salt into the layer for both annual-mean forced and seasonal forced cases. In terms of an evaporative flux this represents about 0.34×10^6 m^3/s or 300 mm/yr of evaporation over the surface of this layer. Another area of high external forcing is the North Atlantic which has 260 mm/yr evaporative flux. The basin which has the highest fresh water input is the Tropical Pacific where there is an input of 116 mm/yr. In comparison, the Atlantic from 15°S to 15°N has a fresh water flux of 70 mm/yr.

Our division of the global ocean into these 8 basins is not the most appropriate for analyzing surface fluxes

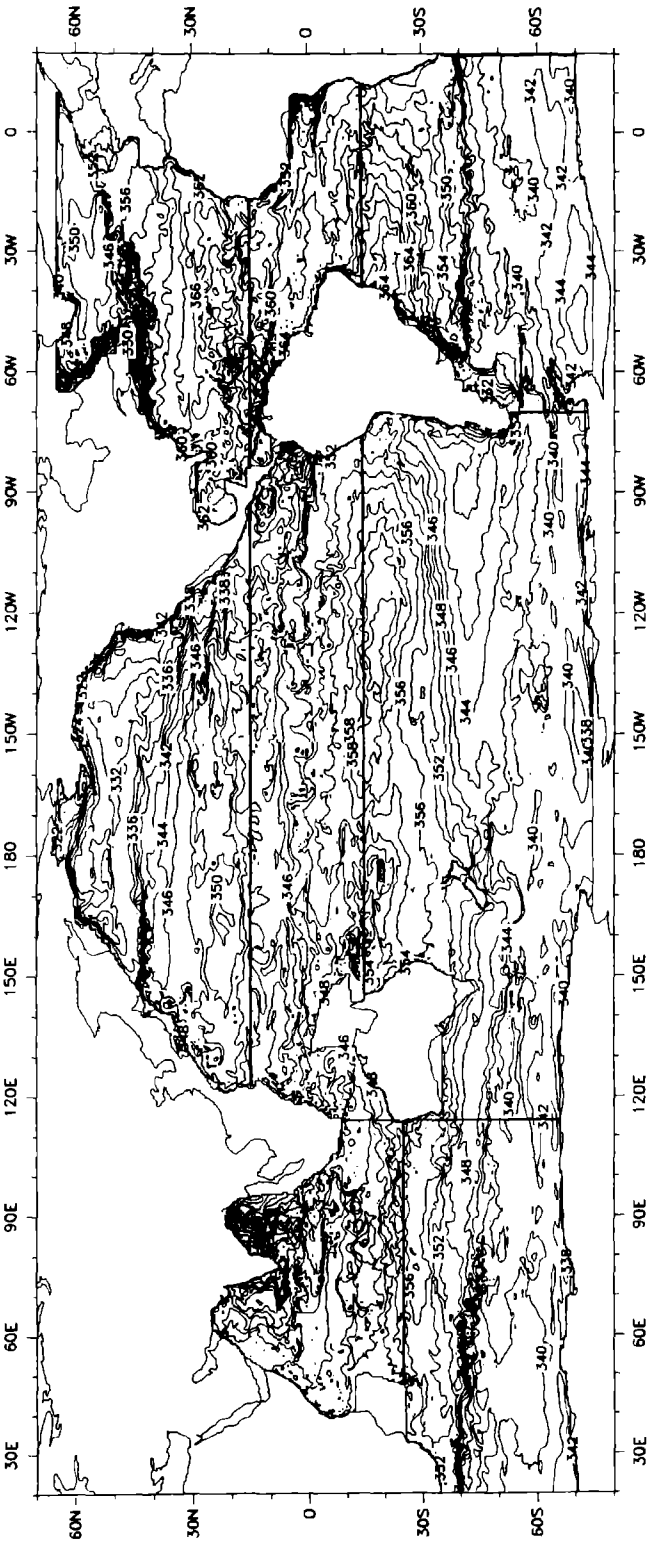

Fig. 11. Salinity at 37.5 m for an instant in early October of year 10 of the seasonal run. Contour interval is 0.2 ppt. Boundaries for the basins used in the budget analysis are indicated

of fresh water. Excess precipitation occurs from the equator to 10°N (the intertropical convergence zone, ITCZ) and mid-latitude excess evaporation extends from the ITCZ to 40°N and to 40°S. Our latitudinal basin boundaries of 15°N and 15°S and the large size

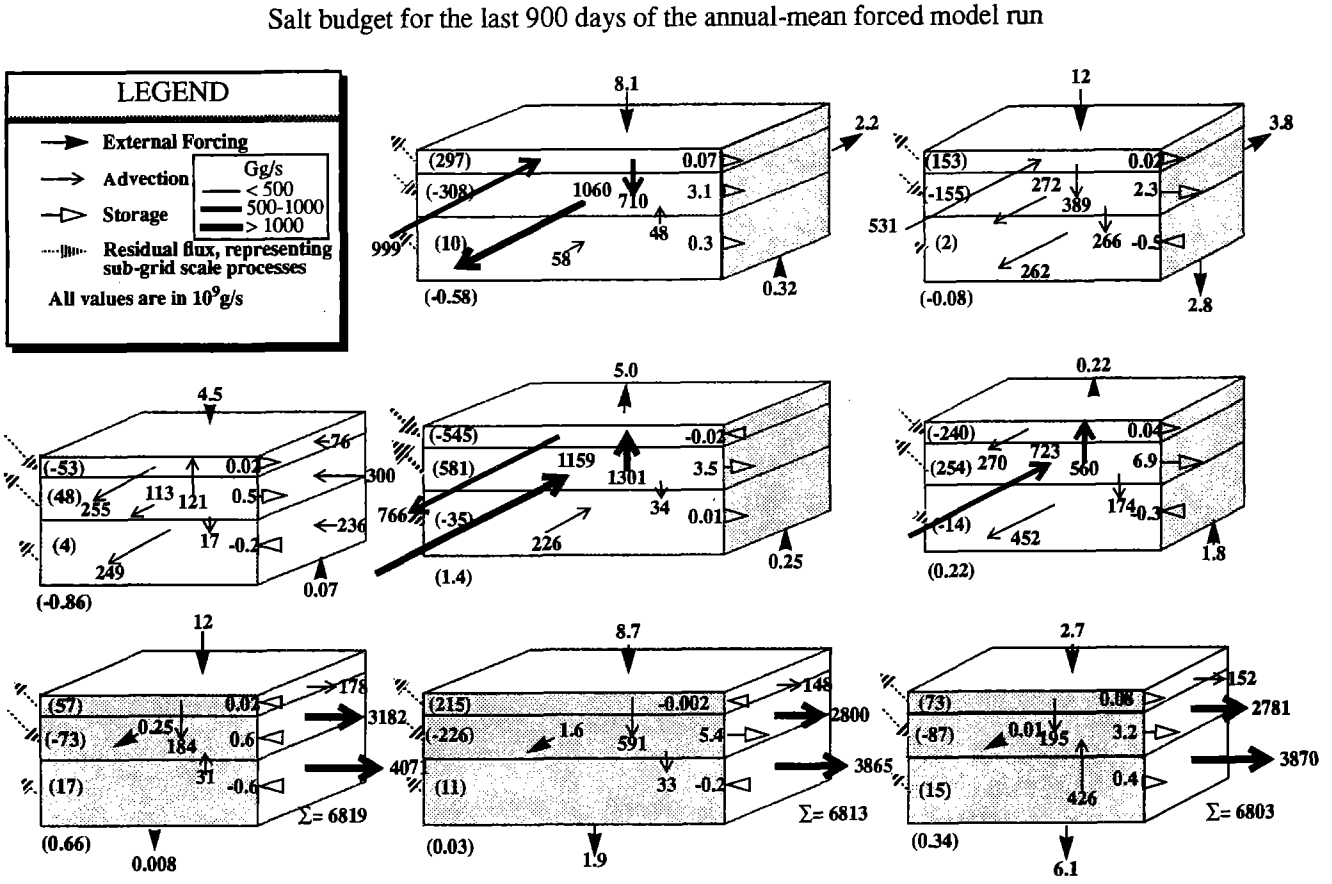

Fig. 12. Salt budget in Gg/s (10^9 g/s) for the last 900 days of the annual-mean forced model run. *Solid filled arrows* represent external forcing, *plain arrows* represent advective transport between layers, *open filled arrows* represent the storage within the layer, and the *broken arrows* represent the sub-grid scale transports into or out of the layer. *Wide arrows* indicate transports greater than 1000 Gg/s, *medium-sized arrows* are for transports between 500 and 1000 Gg/s, and *thin arrows* indicate transports less than 500 Gg/s. The total zonal transports across 113°E, 70°W, and 20°E are shown next to the summation sign near the bottom of the figure

of our basins tend to average out much of these fresh water flux features. Figure 38 in Semtner and Chervin (1992) shows a contour plot of the salinity forcing, indicating areas where there is fresh water forcing of the surface layer. The Tropical Atlantic is visibly freshened by the Amazon River and the Tropical Pacific is freshened by excess precipitation. Excess evaporation takes place in the mid-latitudes with largest values occurring in the South Indian in association with the Agulhas current and its retroflection.

Lateral boundary forcing of salinity is very similar to the external wall forcing of temperature. Everywhere heat is removed from the thermocline, salt is also removed. Deep layer diagnostic forcing is small in all basins except for the North Atlantic and the South Atlantic where salt is removed (fresh water added) by the external forcing. The largest salt forcing is in the deep South Atlantic where 6 Gg/s is removed (a fresh water inflow of 0.17 Sv). The deep layer forcing in the North Atlantic adds 0.11 Sv of fresh water. Fresh water is added to this layer by the diagnostic forcing as a proxy for fresh water input from the Arctic Ocean. In addition, salt is added near the outflow of the Mediterranean in lieu of an actual salty flow.

Storage

The salinity trend in the unforced thermocline layer decreases in all basins but the North Atlantic and North Indian when the forcing was changed from annual-mean to seasonal. As with temperature, the Tropical Atlantic shows the greatest trend, and the trend of the South Atlantic during the last 3 years is opposite to the trend in the other basins. For all basins but the South Indian, salinity in the thermocline increases, which is consistent with the net addition of salt by external forcing. Total external forcing for years 5, 6, and 7 is 19.65 Gg/s; when applied over the global ocean this gives a trend of 0.0047 ppt/decade. Represented as a flux through the surface of the global ocean the average net evaporation is 54 mm/year.

Salt advection

Like heat, salt is transported throughout the ocean by wind and thermohaline driven circulations. For this reason the general nature of salt advection is similar to that of heat advection which has been described above

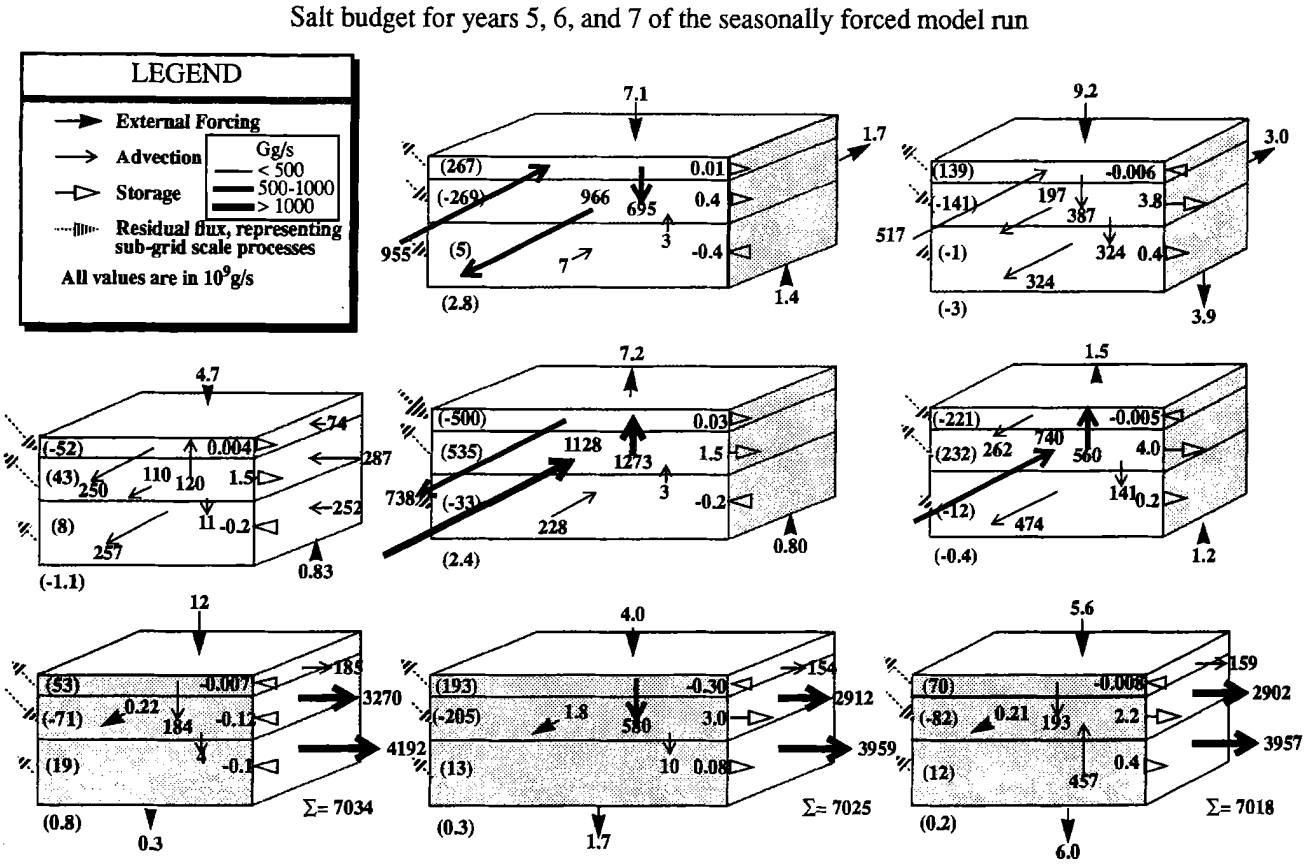

Fig. 13. Salt budget in Gg/s (10^9 g/s) for years 5, 6, and 7 of the seasonally forced model run. Same conventions as Fig. 12

and is shown in Figs. 5, 6, and 7. The salt budget (Figs. 12, 13, and 14) shows a poleward transport away from the equatorial surface layers and a return to the equatorial regions via the thermocline and deep layers. In the North Atlantic there is a nearly equal partition of this flow in these layers across 15°N; whereas in the North Pacific the equatorward salt transport is solely in the thermocline layer. This difference further illustrates the presence of deep water formation with equatorward transport in the North Atlantic and no deep water formation in the North Pacific.

Comparing the zonal transports across 113°E, 70°W and 20°E we see that the Indian loses 16 Gg/s, the Pacific gains 9 Gg/s, and the Atlantic gains 7 Gg/s (Fig. 13). The 7 Gg/s gain in the Atlantic amounts to a fresh water export of 0.20 Sv. The Indian gains 0.46 Sv of fresh water and the Pacific exports about 0.26 Sv. These numbers differ from observational estimates which include the net water transport from the Pacific to the Atlantic via the Arctic Ocean (Baumgartner and Reichel 1975).

Residual fluxes

Figures 13 and 14 show that there is a near balance between the surface and thermocline layer residual fluxes. For salt, the implied sub-grid scale vertical transports are typically about 35% of the advective transports, and they are in the same direction as the advective transports.

As with the residual heat fluxes, we can use the total residual salt flux as an approximate measure of the error in our method. For the annual-mean case the total of the residuals is 1.1 Gg/s. The totals of the residuals for the two samples from the seasonal run are a bit higher: for years 5, 6, and 7 it is 2.5 Gg/s, and for years 8, 9, and 10 it is 2.0 Gg/s. The horizontal diffusive transport of salt is a little less clear than it is for heat. Only the annual-mean run and years 5, 6, and 7 show an implied diffusive transport of fresh water from the North Indian to the South Indian (as would be expected considering the gradient that is seen along the boundary in Fig. 11).

Meridional salt transport and surface fresh water fluxes

Figure 15a shows the depth and latitude integrated salt transports for the global ocean. These transports are computed in the same way as the meridional heat transports which are shown in Fig. 8. Heat is transported away from tropical regions because that is where heat is input to the ocean from the atmosphere. The meridional transport of salt responds in the same way. In southern hemisphere mid-latitudes, salt is transported away from regions of excess evaporation,

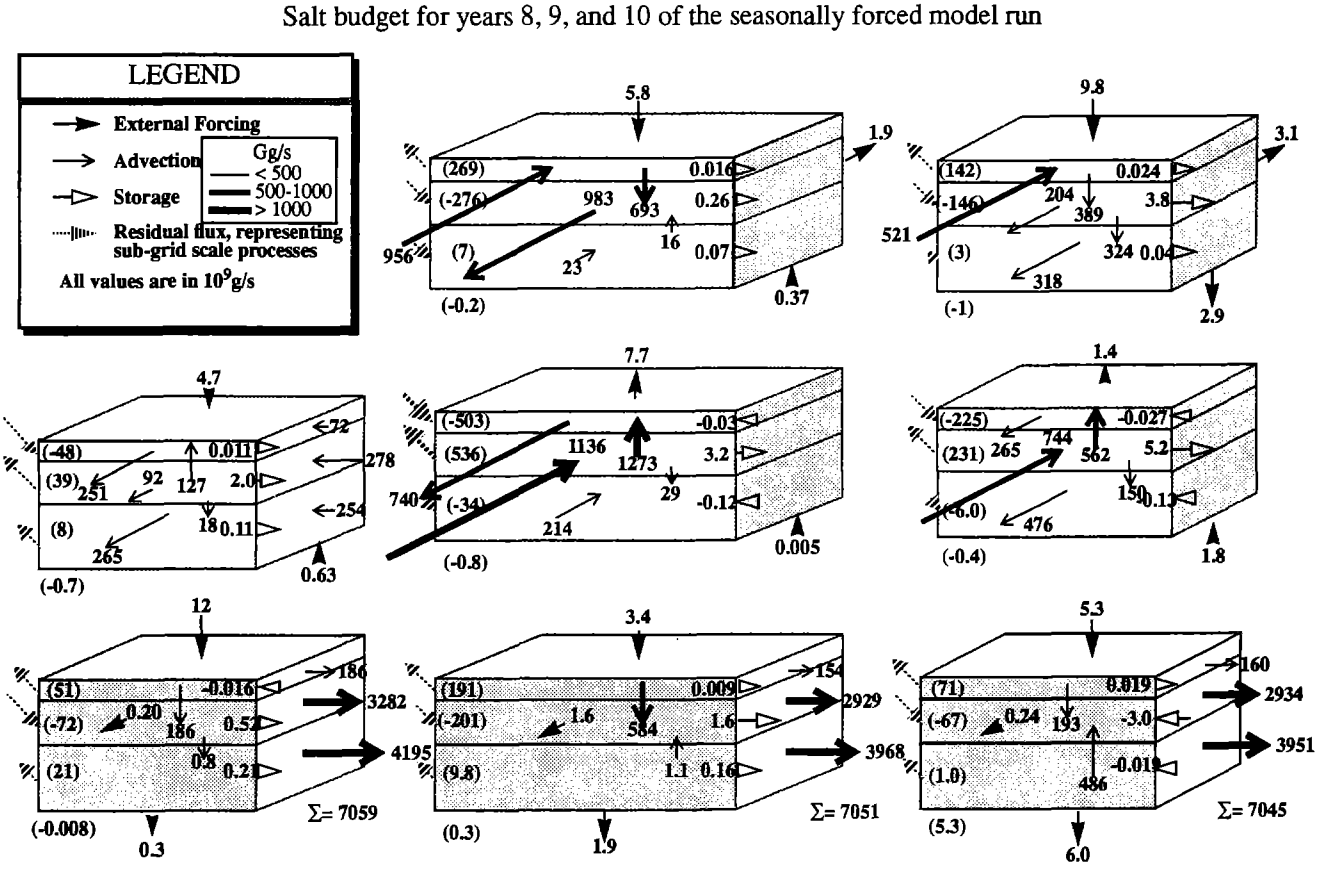

Fig. 14. Salt budget Gg/s (10^9 g/s) for years 8, 9, and 10 of the seasonally forced model run. Same conventions as Fig. 12

much of it occurring in the South Indian Ocean (see Figs. 13 and 14). The Northern hemisphere salt transport is a bit more complex because in the ITCZ (centered at 5°N), a considerable amount of fresh water is added to the ocean. The effect of this in the ocean circulation is a transport of salt toward the ITCZ. In the mid-latitudes, from 15°N to 40°N, evaporation exceeds precipitation and salt is transported poleward.

Eddies in the Pacific vigorously transport salt northward across the equator; whereas in the Atlantic, eddies transport salt southward toward the equator (Figs. 15b and 15c). The stronger Pacific eddy transport is due to the sharper gradient of salinity at the equator caused by the meeting of relatively fresh North Pacific Central Water and the salty Pacific Equatorial Water. The eddy convergence of salt in the Indo-Pacific is quite strong; it amounts to an effective evaporation of 2 m/yr or 0.0024 g/s/m^2 of salt flux (Fig. 16c). This flux of salt at the equator will increase the density of the water, perhaps compensating for the decrease of density caused by the 200 w/m^2 convergence of heat by eddies. A simple calculation using a linear equation of state shows the relative importance of the heat and salt convergences in the equatorial Pacific. The change in near-surface water density ($\Delta\rho$) can be approximated using a linear equation of state:

$$\Delta\rho = \beta\Delta S - \alpha\Delta T,$$

using values of α and β for equatorial surface water and the equatorial peaks of the vertically integrated eddy fluxes from Figs. 10c and 16c, the ratio of the 2 terms on the right hand side is:

$$-\frac{\beta\Delta S}{\alpha\Delta T} = -0.142 \approx -\frac{1}{7}$$

therefore, the heat contributed by eddies in the Pacific contributes 7 parts positive buoyancy for each part of negative buoyancy contributed by the eddy transport of salt.

Much can be revealed by examining the derived surface fresh water fluxes that the circulation of this model requires. Figure 16 shows the total (*solid curves*) and the effective eddy (*dashed curves*) fresh water fluxes for the global, Atlantic, and Indo-Pacific Oceans. These were computed by taking the divergence of the meridional salt transport (Fig. 15) and dividing by -35×10^3 g/m^3. Again, a 2-degree filter was applied, except for the eddy convergences at the equator. Positive values in the total flux indicate a freshening of the ocean by atmospheric or riverine input. Negative values show that evaporation exceeds precipitation and river run-off. The total fresh water flux curve for the Atlantic (Fig. 16b) is similar to observed values shown in Gordon and Piola (1983). The largest deviations are within the ITCZ where the model's fresh water input of 2 m/yr exceeds the value of 1.2 m/yr (determined by a combination of river runoff, evaporation, and precipitation for the Atlantic), and at high latitudes where at 60°N the model's fresh water input of 1 m/yr is about twice the observed value shown in Gordon and

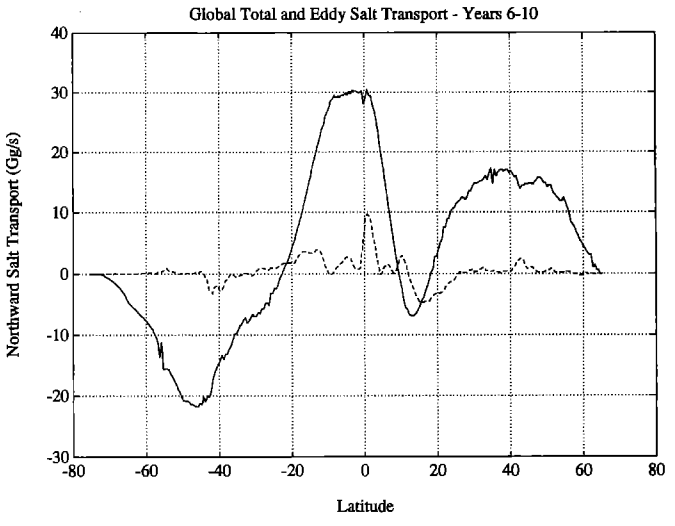

a

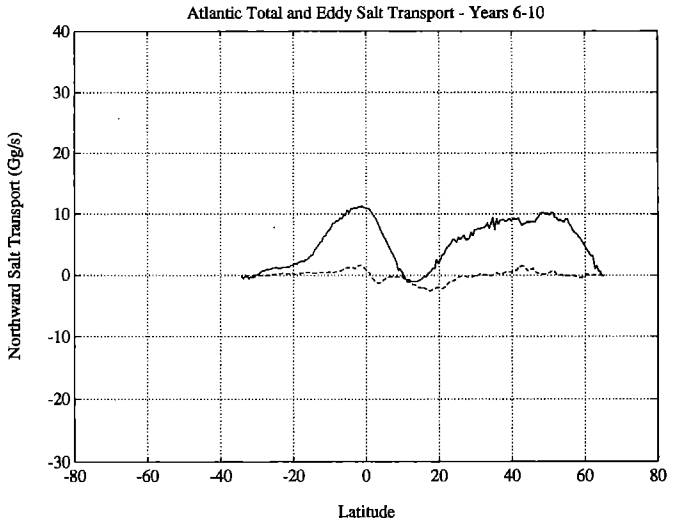

b

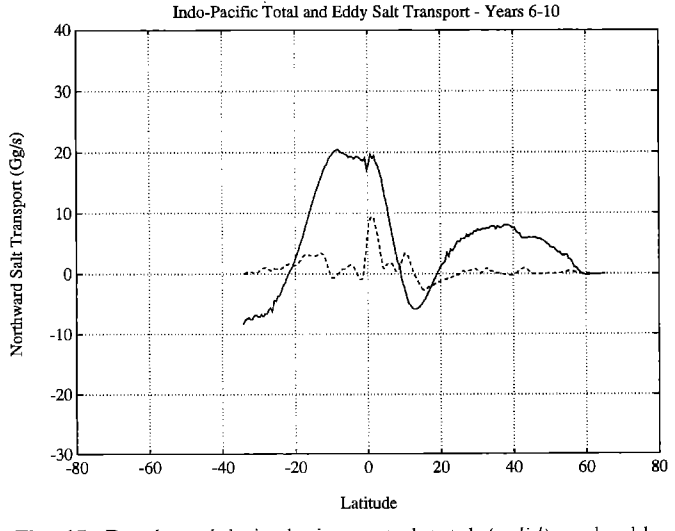

c

Fig. 15. Depth and latitude integrated total (*solid*) and eddy (*dashed*) salt transport in Gg/s (10^9 g/s) over **a** the global ocean **b** the Atlantic ocean, and **c** the Indo-Pacific ocean

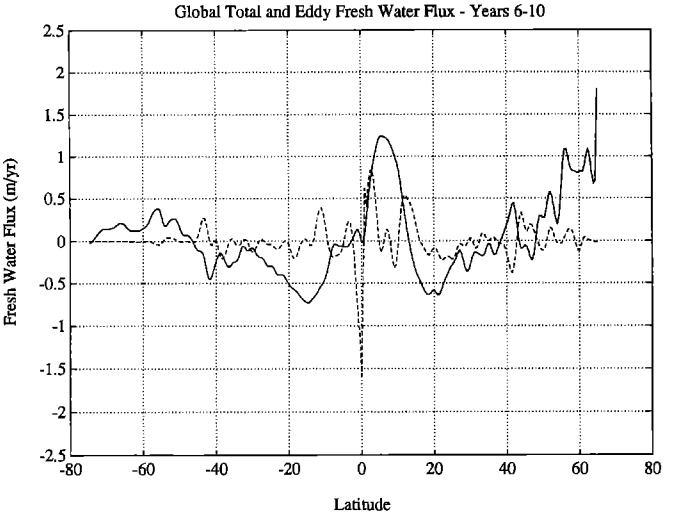

a

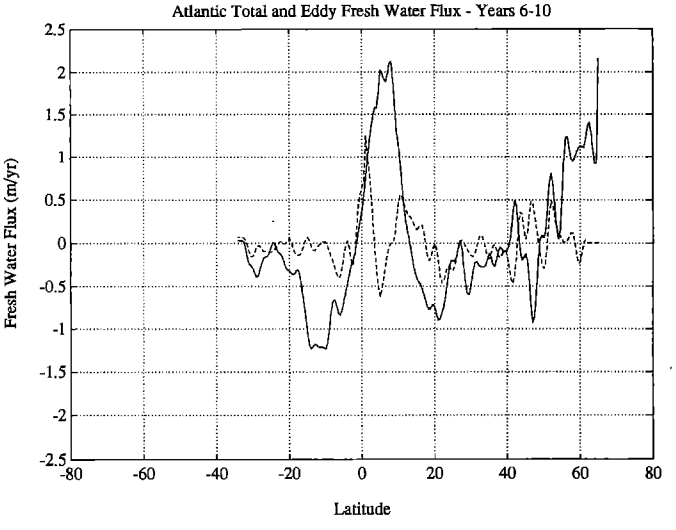

b

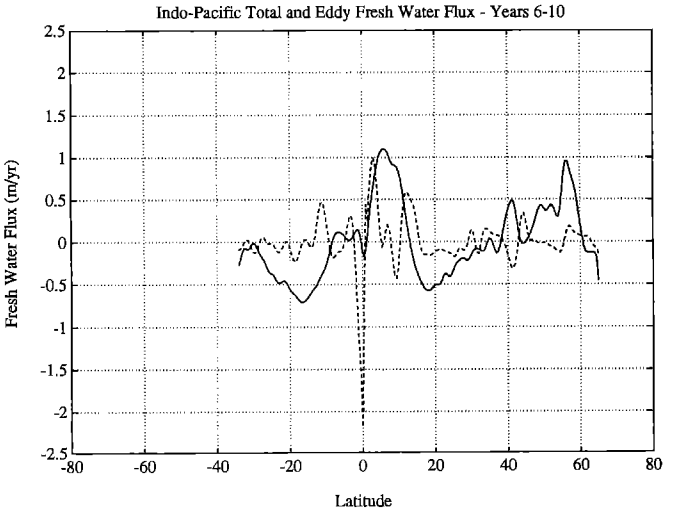

c

Fig. 16. Derived total (*solid*) and eddy (*dashed*) fresh water flux in m/year over **a** the global ocean, **b** the Atlantic ocean, and **c** the Indo-Pacific ocean. The *solid line* represents the surface fresh water flux required by the model's circulation (positive values mean fresh water is added to the ocean) and the *dashed line* represents the effective fresh water flux due to eddies (positive values mean that the eddies converge fresh water in the ocean)

Piola's figure. The total fluxes for the Indo-Pacific (Fig. 16c) show a similar pattern to the Atlantic, but the extremes are about half the magnitude and the fresh water influx does not extend to the northern boundary.

Oceanic fresh water transport

Wijffels et al. (1992) discuss the importance of the fresh water transport from the Pacific to the Atlantic via the Arctic Ocean. This model has no Arctic Ocean and the wall forcing at the northern boundaries is an inadequate substitute for the flow that occurs there. For instance, the diagnostic forcing at the North Pacific wall introduces 0.049 Sv of fresh water into the Pacific. This is opposite to what is observed by Coachman and Aagaard (1988). They measured a 0.8 Sv flow of relatively fresh, 32.5 ppt, water flowing from the Pacific to the Arctic. This is a 0.77 Sv transport of fresh water out of the Pacific. Adding the net fresh water input that occurs in the Arctic, the flux of fresh water into the Atlantic from the Arctic is 0.95 Sv. Wall forcing in the model's North Atlantic adds only 0.09 Sv of fresh water and deep layer forcing adds only another 0.08 Sv (Fig. 14).

The model's fresh water transport can be calculated from Fig. 15 by dividing by 35×10^3 g/m^3 and reversing the sign. This is valid because in the model the meridional mass transport is zero along these curves. For the Atlantic and Indo-Pacific basins we can adjust the fresh water transports by adding the known fresh water exchange with the Arctic Ocean. Figure 17 shows these adjusted fresh water transports for the global, Atlantic, and Indo-Pacific oceans (*solid curves*). The observed transports, computed by integrating Baumgartner and Reichel's (1975, Table XXXV) fresh water flux data along the 5 degree latitude bands, are shown as *dashed curves* with *asterisks* in Fig. 17. The model's transport integrated over the globe (Fig. 17a) compares quite well with the inferred transport computed from surface fluxes. It is also a good complement to atmospheric water vapor transport (*dotted curves* with *circles*, Fig. 17a) as inferred from radiosonde observations by Peixóto and Oort (1983). The Indo-Pacific transport also compares quite well with the observed data (Fig. 17c). However, in the Atlantic, the model transports too much fresh water southward, or too much salty water northward (Fig. 17b). The absence of an actual flow of salty Mediterranean water, and a weak northward flow of relatively fresh Antarctic Intermediate Water (AAIW) probably contribute to this difference.

The observed salt flux into the Atlantic from the Mediterranean is only about 1.5 Gg/s according to Bryden and Kinder (1991). Its effect in the model could be increased by explicitly including the Mediterranean or by strengthening the diagnostic forcing near its outflow. The most we could decrease the model's excess southward transport would be about 0.04 Sv (1.5 Gg/s divided by -35×10^3 g/m^3), whereas the discrepancy with observations is about 0.5 Sv.

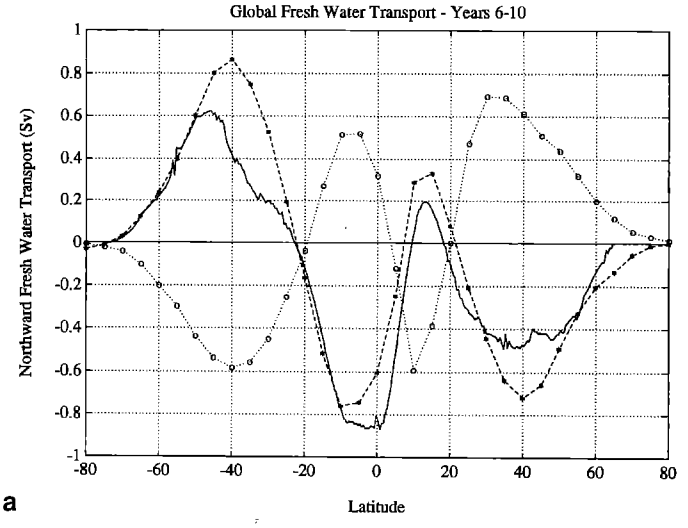

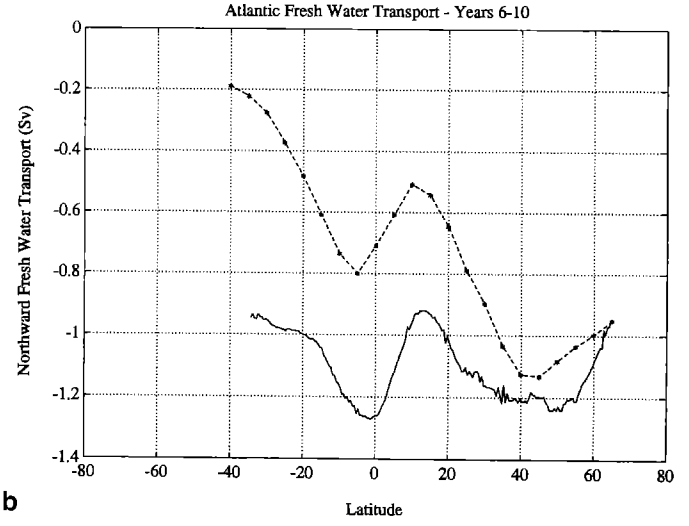

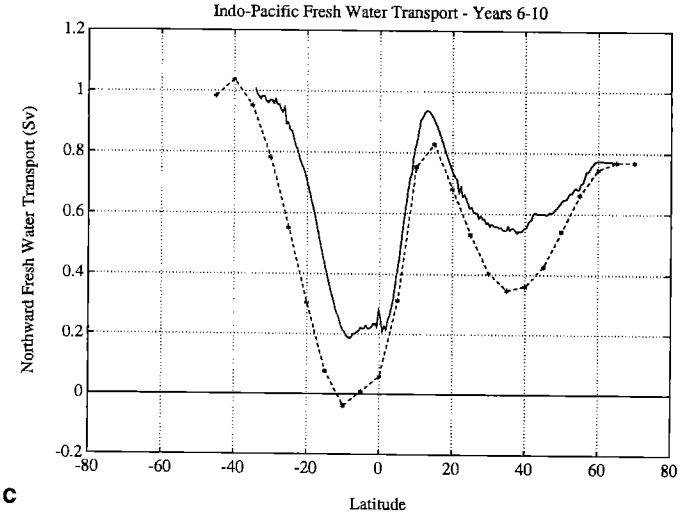

Fig. 17. Oceanic fresh water transports in 10^6 m^3/s computed from the model's circulation (*solid*) and inferred from Baumgartner and Reichel's (1975) fresh water flux tabulation (*dashed*) over **a** the global ocean (atmospheric water vapor transport from Peixóto and Oort, 1983, is shown as a *dotted curve with circles*), **b** the Atlantic Ocean, and **c** the Pacific Ocean

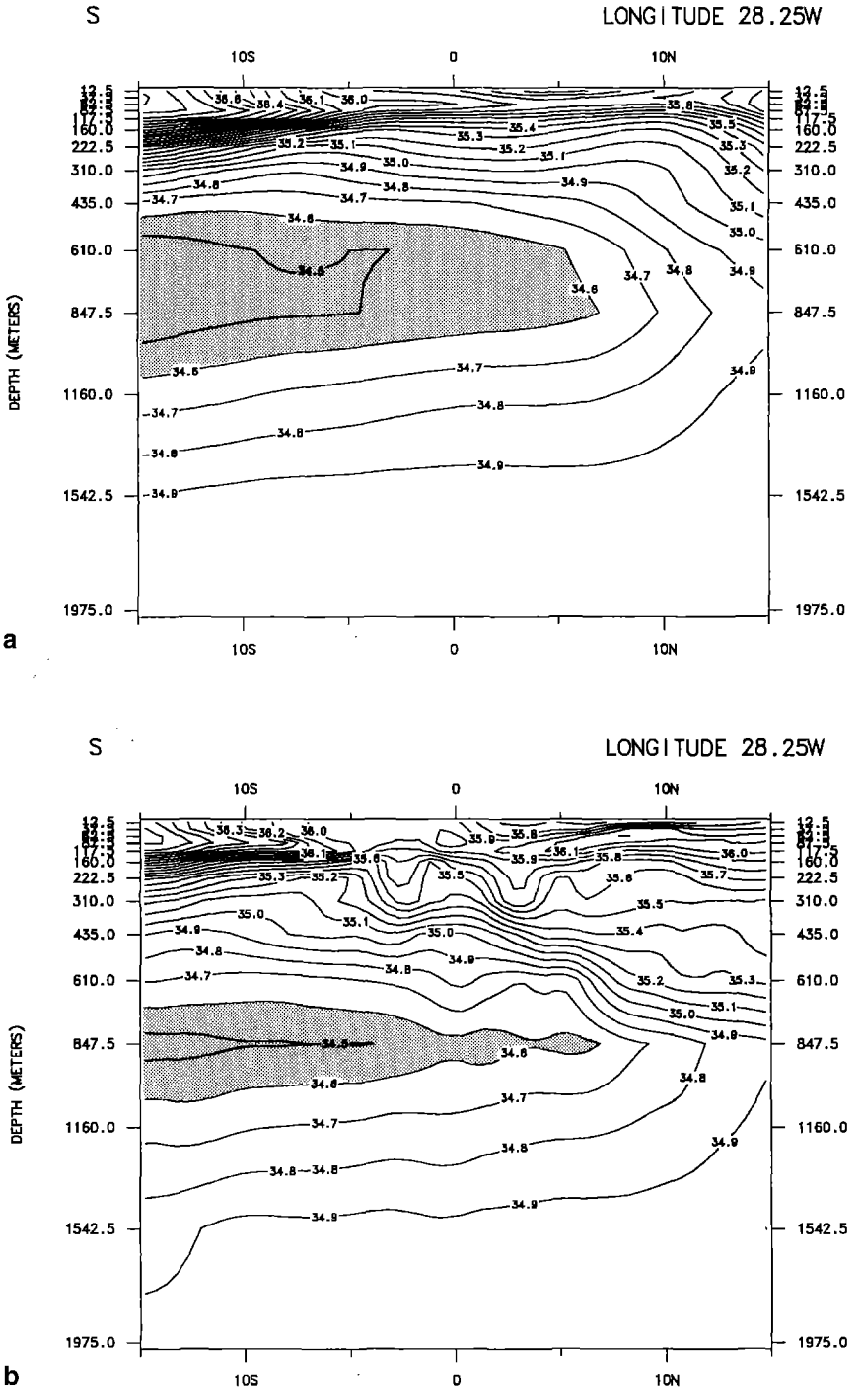

Fig. 18. Meridional section of salinity along 28° W in the Atlantic from **a** Levitus (1982) data set and from **b** years 6 through 10 of the seasonal run. While the model unsmoothed the Levitus data in the surface levels it shrunk the volume of AAIW

A more likely explanation for the model's disagreement with observations is the model's inadequate flow of AAIW. Figure 18a is a meridional section of salinity from the Levitus (1982) historical data set along 28° W; Fig. 18b is the same section from the mean of last five years of the seasonal run. Note the 34.60 halocline: the Levitus data show it enclosing about 400 m of fresher water at the latitude of the equator, whereas the model encloses only about 100 m of fresher water. Because much of the AAIW circulation is within the model's unrestrained thermocline layer, the volume of fresh water has been reduced by a combination of poor resolution of the intermediate water formation process and perhaps because of a low salinity bias in the Levitus surface forcing data. (See England, 1992, for a discussion on the importance of surface salinity forcing in the formation of southern hemisphere intermediate and bottom water.) Better agreement with observations can be expected when the Arctic domain, the Mediterranean outflow, and better southern hemisphere forcing fields are included in a higher resolution implementation of this model.

7 Summary

The partitioning of the ocean into regional basins has given us an overall view of the forcing, trends, and transports of this model. Changing the external forcing from annual-mean to seasonally-varying, strengthened NADW formation to a rather realistic value of 14 Sv. Free thermocline layer trends and deep layer robust-diagnostic forcing also improved with the introduction of seasonal forcing. Volume transports of the ACC and of the Indonesian passage throughflow exceed measured values by about 30%. Weak Antarctic Intermediate and Bottom Water formation probably contributes to an anomalous equatorward transport of heat in the southern hemisphere, and causes an overestimation of the southward transport of fresh water in the Atlantic. Improvements that will increase AAIW and AABW formation are needed to create a more realistic simulation of the global thermohaline circulation. These changes are necessary if this model is to be used for simulating and offering predictions of global climate change. The intermediate and bottom water formation problems in this model also point to possible problems in coarse resolution climate models which perhaps rely too heavily on lateral diffusion to transport heat poleward, and hence gloss over the actual mechanisms of oceanic transport.

An analysis of the residuals left over from summing the known fluxes into each volume shows the magnitude of the sub-grid scale processes. In terms of transporting heat and salt, vertical mixing processes are more important than horizontal diffusion. The subgrid scale temperature transports between the surface and thermocline layers are typically about 25% of the advective transports, for salt the percentage is about 35%. These indirect measures of mixing are marginally useful; to assess accurately the effects of mixing on vertical transports and water mass formation, we must know the actual mixing within each model cell. A count of how often each cell is mixed should be recorded in future history tape archives.

The zonally integrated surface heat and fresh water fluxes that the circulation of this model requires give an indication of the role eddies play in the meridional transport of heat and fresh water. Eddies act to redistribute heat or fresh water that is added by surface forcing. The greatest possible effect of eddies on the global circulation is in the Tropical Pacific where tropical instability waves converge heat and buoyancy toward the equator. Perhaps the most important climatological effect of eddies is their role in adding buoyancy to the upwelling portion of the global conveyor-belt circulation.

This is the first global model that is able to resolve eddies (albeit marginally in the mid- and high-latitudes). By limiting the number of open boundaries in this simulation we eliminate may of the "side-effects" which can contaminate an analysis of fluxes between ocean basins on a global scale. The future is encouraging for high-resolution global ocean modeling. Massively parallel supercomputers will make possible a doubling of this model's horizontal and vertical resolution. High latitude eddies will be better resolved and convection may improve as the model's grid approaches the actual scales of the deep convective process. However, better estimates of the surface temperature and salinity boundary conditions will be needed to construct a more realistic simulation of the thermohaline circulation.

Acknowledgements. The authors thank Tom Bettge at NCAR for maintaining the Ocean Processor program and for helping with its modifications. Friendly critical review of this manuscript was provided by Tom Murphree of the Naval Postgraduate School. An anonymous reviewer is also thanked for several worthwhile suggestions. The first two authors of this paper were supported by Grants ATM-8705980 and OCE-8812472 from the National Science Foundation and by Contract No. 079067-A-B1 from Battelle Pacific Northwest Laboratories of the United States Department of Energy. Support from the NSF Physical Oceanography Program was for modeling related to the World Ocean Circulation Experiment. The third author was partially supported by a Department of Energy grant from the Carbon Dioxide Research Program to NCAR. Computing resources were provided by the Scientific Computing Division of the National Center for Atmospheric Research. NCAR is sponsored by the National Science Foundation.

References

Baumgartner A, Reichel E (1975) The world water balance. Elsevier, New York

Bennett AF (1978) Poleward heat fluxes in southern hemisphere oceans. J Phys Oceanogr 8:785–798

Bryan K (1969) A numerical model for the study of the world ocean. J Comput Phys 4:347–376

Bryan K (1991) Poleward heat transport in the ocean. A review of a hierarchy of models of increasing resolution. Tellus 43AB:104–115

Bryan FO, Holland WR (1989) A high resolution simulation of the wind- and thermohaline-driven circulation in the North Atlantic Ocean. Proceedings 'Aha Huliko' a, Hawaii Institute of Geophysics Special Publication

Bryden HL, Brady EC (1989) Eddy momentum and heat fluxes and their effects on the circulation of the equatorial Pacific Ocean. J Mar Res 47:55–79

Bryden HL, Kinder TH (1991) Recent progress in strait dynamics. IUGG US National report, AGU

Carissimo BC, Oort AH, Vonder Haar TH (1985) Estimating the meridional energy transports in the atmosphere and ocean. J Phys Oceanogr 15:82–91

Chervin RM, Semtner AJ (1990) An ocean modeling system for supercomputer architectures of the 1990's. In: Schlesinger M (ed) Proceedings of the NATO Advanced Research Workshop on Climate-ocean interaction. Kluwer, Dordrecht, pp 87–95

Coachman LK, Aagaard K (1988) Transports through Bering Strait: annual and interannual variability. J Geophys Res 93:15535–15539

Cox MD (1975) A baroclinic numerical model of the world ocean: preliminary results. Numerical models of ocean circulation. National Academy of Sciences, Washington DC, pp 107–118

England MH (1992) On the formation of Antarctic Intermediate and Bottom Water in ocean general circulation models. J Phys Oceanogr 22:918–926

Fine RA (1985) Direct evidence using tritium data for throughflow from the Pacific into the Indian Ocean. Nature 315:478–480

FRAM Group (1991) An eddy-resolving model of the southern Ocean. EOS, Trans Am Geophys Union 72:169 and 174–175

Fugio S, Imasoto N (1991) Diagnostic calculation for circulation and water mass movement in the deep Pacific. J Geophys Res 96:759–774

Godfrey JS (1989) A Sverdrup model of the depth-integrated flow for the ocean allowing for island circulations. Geophys Astrophys Fluid Dynamics 45:89–112

Gordon AL (1986) Interocean exchange of thermocline water. J Geophys Res 91:5037–5046

Gordon AL, Piola AR (1983) Atlantic ocean upper layer salinity budget. J Phys Oceanogr 13:1293–1300

Hall MM, Bryden HL (1982) Direct estimates and mechanisms of ocean heat transport. Deep-Sea Res 29:339–359

Hastenrath S (1982) On meridional heat transports in the world ocean. J Phys Oceanogr 12:922–927

Hastenrath S, Lamb P (1977) Climate atlas of the tropical Atlantic and eastern Pacific oceans. University of Wisconsin Press, Wisconsin

Kindle JC, Heburn GW, Rhodes RC (1987) An estimate of the Pacific to Indian Ocean throughflow from a global numerical model. In: Katz EJ, Witte JM (eds) Further progress in equatorial oceanography. Nova University Press, Ft. Lauderdale, Florida, pp 317–321

Legeckis RV (1977) Long waves in the eastern equatorial Pacific Ocean: a view from a geostationary satellite. Science 197:1179–1181

Levitus S (1982) Climatological atlas of the world oceans. Nat Ocean Atmos Adv Prof Pap 13, US Government Printing Office, Washington DC

Long EC (1990) Analysis of an eddy-resolving global ocean model in the tropical Indian Ocean. Masters Thesis NPS-68-90-008, Naval Postgraduate School, Monterey, Calif.

Maier-Reimer E, Mikolajewicz U (1989) Experiments with an OGCM on the cause of the Younger Dryas. In: Ayala-Castanares A, Wooster W, Yanez-Arancibia A (eds) Oceanography. UNAM Press, Mexico DF, pp 87–100

Masamichi I, Welsh SE (1990) Seasonal and interannual variability in the Indo-Pacific throughflow. Trans Am Geophys Union 71:1397

Pacanowski RC, Philander SGH (1981) Parameterization of vertical mixing in numerical models of tropical oceans. J Phys Oceanogr 11:1443–1451

Peixóto JP, Oort AH (1983) The atmospheric branch of the hydrological cycle and climate. In: Street-Perrott A, Beran M, Ratcliffe R (eds) Variations in the global water budget. Reidel, Dordrecht, pp 5–65

Piola AR, Gordon AL (1984) Pacific and Indian Ocean upper-layer salinity budget. J Phys Oceanogr 14:747–751

Roemmich D (1983) The balance of geostrophic and Ekman transports in the tropical Atlantic Ocean. J Phys Oceanogr Res 13:1534–1539

Sarmiento JL (1986) On the north and tropical Atlantic heat balance. J Geophys Res 91:11677–11689

Semtner AJ (1986a) History and methodology of modelling the circulation of the world ocean. In: O'Brien JJ (ed) Advanced physical oceanographic numerical modelling. D Reidel, Norwell, Mass, pp 23–32

Semtner AJ (1986b) Finite-difference formulation of a world ocean model. In: O'Brien JJ (ed) Advanced physical oceanographic numerical modelling, D Reidel, Norwell, Mass, pp 187–202

Semtner AJ, Chervin RM (1988) A simulation of the global ocean circulation with resolved eddies. J Geophys Res 93:15502–15522 and 15767–15775

Semtner AJ, Chervin RM (1992) Ocean general circulation from a global eddy-resolving model. J Geophys Res 97:5493–5550

Stommel H, Arons AB (1960) On the abyssal circulation of the world ocean – II. An idealized model of the circulation pattern and amplitude in oceanic basins. Deep-Sea Res 6:217–233

Whitworth T III, Nowlin WD Jr (1987) Water masses and currents of the southern ocean at the greenwhich meridian. J Geophys Res 92:6462–6476

Whitworth T III, Nowlin WD Jr, Worley SJ (1982) The net transport of the Antarctic circumpolar current through Drake Passage. J Phys Oceanogr 12:960–971

Woods J (1985) The world ocean circulation experiment. Nature 314:501–511

Wunsch C, Hu D, Grant B (1983) Mass, heat, salt, and nutrients fluxes in the South Pacific Ocean. J Phys Oceanogr 13:725–753

Wijffels SE, Schmitt RW, Bryden HL, StTigebrandt A (1992) On the transport of freshwater by the oceans. J Phys Oceanogr 22:155–162